Homogeneous studies of transiting extrasolar planets. III. Additional planets and stellar models

John Southworth[*]

Astrophysics Group, Keele University, Staffordshire, ST5 5BG, UK

24 June 2010

ABSTRACT

I derive the physical properties of thirty transiting extrasolar planetary systems using a homogeneous analysis of published data. The light curves are modelled with the JKTEBOP code, with special attention paid to the treatment of limb darkening, orbital eccentricity, and error analysis. The light from some systems is contaminated by faint nearby stars, which if ignored will systematically bias the results. I show that it is not realistically possible to account for this using only transit light curves: light curve solutions must be constrained by measurements of the amount of contaminating light. A contamination of 5% is enough to make the measurement of a planetary radius 2% too low.

The physical properties of the thirty transiting systems are obtained by interpolating in tabulated predictions from theoretical stellar models to find the best match to the light curve parameters and the measured stellar velocity amplitude, temperature and metal abundance. Statistical errors are propagated by a perturbation analysis which constructs complete error budgets for each output parameter. These error budgets are used to compile a list of systems which would benefit from additional photometric or spectroscopic measurements.

The systematic errors arising from the inclusion of stellar models are assessed by using five independent sets of theoretical predictions for low-mass stars. This model dependence sets a lower limit on the accuracy of measurements of the physical properties of the systems, ranging from 1% for the stellar mass to 0.6% for the mass of the planet and 0.3% for other quantities. The stellar density and the planetary surface gravity and equilibrium temperature are not affected by this model dependence. An external test on these systematic errors is performed by comparing the two discovery papers of the WASP-11 / HAT-P-10 system: these two studies differ in their assessment of the ratio of the radii of the components and the effective temperature of the star.

I find that the correlations of planetary surface gravity and mass with orbital period have significance levels of only 3.1σ and 2.3σ, respectively. The significance of the latter has not increased with the addition of new data since Paper II. The division of planets into two classes based on Safronov number is increasingly blurred. Most of the objects studied here would benefit from improved photometric and spectroscopic observations, as well as improvements in our understanding of low-mass stars and their effective temperature scale.

Key words: stars: planetary systems — stars: binaries: eclipsing — stars: binaries: spectroscopic — stars: fundamental parameters

1 INTRODUCTION

The study of extrasolar planets is scientifically and culturally important, and after a late start (Mayor & Queloz 1995) the number of known planets is escalating rapidly[1]. Transiting planets are the crown jewels of this population as, with the exception of our own Solar system, they are the only planets whose masses and radii are directly measurable. In addition to this, it is possible to put con-

straints on the properties of their atmospheres, in which much interesting physics occurs, through measurements of the depths of transits and occultations at different wavelengths.

Whilst transiting extrasolar planets (TEPs) offer unique scientific possibilities, their study involves several complications. The most significant is that it is not in general possible to measure the mass and radius of a planet through basic observations alone. Additional constraints are needed, and are usually provided by forcing the properties of the host stars to match theoretical expectations[2].

---

[*] E-mail: jkt@astro.keele.ac.uk
[1] see the Extrasolar Planets Encyclopædia, http://exoplanet.eu/

[2] In principle, astrometric observations could either replace radial velocity

This introduces not only a model dependence (i.e. systematic error), but also the possibility of inconsistent results if different theoretical predictions are used for some TEPs. Systematic errors can blur any distinctions between planets, making it hard to pick out discrete groups of TEPs from the varied general population.

This systematic error cannot be abolished, but it can at least be standardised. In this series of papers I am analysing the known transiting systems using rigorously homogeneous methods, with the aim of removing the systematic differences in measurements of the physical properties of TEPs. The resulting physical properties are therefore statistically compatible, and any structure in distributions of parameters is maximised.

In Paper I (Southworth 2008) I analysed the light curves of the fourteen transiting systems for which high-precision photometry was then available, paying careful attention to the role of limb darkening and to the estimation of comprehensive errorbars. Paper II (Southworth 2009) used these results plus the predictions of three different theoretical stellar models to measure the physical properties of the fourteen TEPs. In this work I broaden the analysis to thirty TEPs and five sets of theoretical stellar models, resulting in improved statistics and better systematic error estimates.

There are a few homogeneous analyses of transiting systems available in the literature. A good analysis of 23 systems was presented by Torres et al. (2008, hereafter TWH08), but these authors tried only two different theoretical model sets and did not assign systematic errors to their results. Analogously, such work would also benefit from homogeneous analysis of the spectra of the host stars in order to put their effective temperature and chemical abundance measurements on a consistent scale. Steps towards this goal were pioneered by Valenti & Fischer (2005) and are being continued by Ammler-von Eiff et al. (2009) and Ghezzi et al. (2010), but a homogeneous study of the host stars of all known TEPs is not currently available.

In Sect. 2 I present the methods used to analyse the light curves of the thirty TEPs included in this work. Sect. 3 discusses the five theoretical stellar model sets and their application to determining the physical properties of the TEPs. Sect. 4 presents the new results for these objects, Sect. 5 discusses the influence of systematic errors due to the use of theoretical models, and in Sect. 6 I summarise the physical properties of the known TEPs and explore correlations between various parameters. Those readers interested in the general properties of TEPs rather than specific systems can skip Sect. 4 without problem.

2   LIGHT CURVE ANALYSIS: JKTEBOP

I have modelled the light curves of each TEP using the JKTE-BOP[3] code (Southworth et al. 2004a,b). JKTEBOP grew out of the original EBOP program written for eclipsing binary star systems (Popper & Etzel 1981; Etzel 1981) and implementing the NDE model (Nelson & Davis 1972). JKTEBOP uses biaxial spheroids to model the component stars (or star and planet) so allows for departures from sphericity. The shapes of the components are governed by the mass ratio, q, although the results in this work are all extremely insensitive to the value of this parameter.

The main parameters of a JKTEBOP fit are the orbital inclination, i, and the fractional radii of the two stars[4], r_A and r_b. The fractional radii are defined as

$$r_A = \frac{R_A}{a} \qquad\qquad r_b = \frac{R_b}{a} \qquad\qquad (1)$$

where R_A and R_b are the stellar and planetary radii and a is the orbital semimajor axis. r_A and r_b correspond to radii of spheres of the same volume as the biaxial spheroids. In JKTEBOP the fractional radii are re-parameterised as their sum and ratio:

$$r_A + r_b \qquad\qquad k = \frac{r_b}{r_A} = \frac{R_b}{R_A} \qquad\qquad (2)$$

because these are only weakly correlated with each other. In general the orbital period, P_{orb}, is taken from the literature and the time of transit midpoint, T_0, is included as a fitted parameter in each JKTEBOP run.

2.1   Treatment of limb darkening

The limb darkening (LD) of the star is an important 'nuisance parameter' affecting transit light curves which can be parametrised using any of five LD laws in JKTEBOP. Wherever possible the LD coefficients are included as fitted parameters, but when there is insufficient information for this the coefficients are fixed at theoretical values. For each light curve I have obtained solutions with each of the five LD laws (see Paper I for their definition) and with both LD coefficients fixed, with the linear coefficient fitted and the nonlinear coefficient fixed (hereafter referred to as 'LD fit/fix'), and with both coefficients fitted.

Theoretical LD coefficients have been taken from Van Hamme (1993), Claret (2000, 2004a) and Claret & Hauschildt (2003). The tabulated values have been bilinearly interpolated, using the JKTLD code[5], to the known effective temperature (T_{eff}) and surface gravity ($\log g$) of the star. I find that there is usually a spread of 0.1–0.2 in the theoretical LD coefficients for cool stars, so when the nonlinear LD coefficient is not included as a fitted parameter it is perturbed in the Monte Carlo simulations by ± 0.1 on a flat distribution to account for this. The dependence on theoretical calculations in this case is still exceptionally small, because the linear and nonlinear coefficients of the LD laws are highly correlated with each other (Southworth et al. 2007a).

Once solutions have been obtained for the five LD laws, the final result is calculated by taking the weighted means of the parameter values for the four two-parameter LD laws (i.e. the linear law is not used). The parameter errorbars are taken to be the largest of the individual errorbars (see below) plus a contribution to account for scatter of the parameter values from different LD law solutions.

2.2   Error analysis

For each solution I run 1000 Monte Carlo simulations (Southworth et al. 2004c, 2005) to provide robust estimates of the 1σ statistical errorbars. The starting parameter values are perturbed

---

measurements, or augment them and thus provide the missing constraint, but this has not yet been achieved in practise.

[3] JKTEBOP is written in FORTRAN77 and the source code is available at http://www.astro.keele.ac.uk/~jkt/codes/jktebop.html

[4] Throughout this work stellar parameters are indicated by a subscripted 'A' and planet parameters by a subscripted 'b', to conform to IAU nomenclature.

[5] JKTLD is written in FORTRAN77 and the source code is available at http://www.astro.keele.ac.uk/~jkt/codes/jktld.html

for each simulation to avoid sticking artificially close to the original best fit. If the reduced χ^2 of the fit, χ^2_ν, is greater than unity, the Monte Carlo errorbars are multiplied by $\sqrt{\chi^2_\nu}$ to account for this.

Monte Carlo simulations do not fully account for the presence of correlated ('red') noise, which is an unavoidable reality in high-precision light curves of bright stars. I therefore also run a residual permutation (or "prayer bead") algorithm (Jenkins et al. 2002) with the quadratic LD law. If there is significant correlated noise the residual-permutation errorbars will exceed the Monte-Carlo errorbars. I then take the larger of the two error estimates to represent the final errorbars of the photometric parameters.

2.3 Orbital eccentricity

Some TEPs have a non-circular orbit which must be accounted for in the light curve analysis. Orbital eccentricity is very difficult to detect from the shape of a transit light curve (Kipping 2008) but can have a significant effect on the resulting parameters (for an example see Sect. 4.13). Non-circular orbits normally become apparent from radial velocity (RV) measurements of the parent stars. These RVs can then be used to determine the eccentricity, e, and the longitude of periastron, ω, of the binary orbit.

JKTEBOP has been modified to account for orbital eccentricity by including the possibility of specifying values for either e and ω or the combinations $e\cos\omega$ and $e\sin\omega$. These values and their uncertainties are then simply treated as extra observations, and e and ω (or their combinations) are included as fitted parameters. In this way the uncertainties in e and ω are correctly propagated into the errorbars in the other photometric parameters. I prefer to work with $e\cos\omega$ and $e\sin\omega$ rather than e and ω, because the latter two quantities are strongly correlated with each other (e.g. Bruntt et al. 2006).

2.4 Contaminating light

It is possible for additional light to contaminate photometric observations of transiting planets. Any extra light from nearby faint stars will dilute the transit depth, causing a systematic error in the light curve parameters. This idea is becoming more important for several reasons. Firstly, the CoRoT satellite has a large point spread function (PSF) which usually contains a number of stars aside from the one hosting a transiting planet. Secondly, observations using telescope defocussing are potentially more susceptible to contaminating light. Thirdly, Daemgen et al. (2009) have detected faint companions to three transiting systems (TrES-2, TrES-4 and WASP-2) from ground-based high-resolution observations of fourteen TEPs obtained with a lucky-imaging camera. These companions could be bound to their respective transiting systems, or may just be asterisms.

Temporarily ignoring the orbital ephemeris (P_{orb} and T_0), there are three main observables in a transit shape: its depth, duration, and the duration of totality (Paper I). From transit light curves we measure three quantities, which in the case of JKTEBOP are r_A, r_b and i. It is therefore expected to be impossible to fit directly for contaminating light, as this would require measuring four independent parameters using only three observables. This expectation will now be verified.
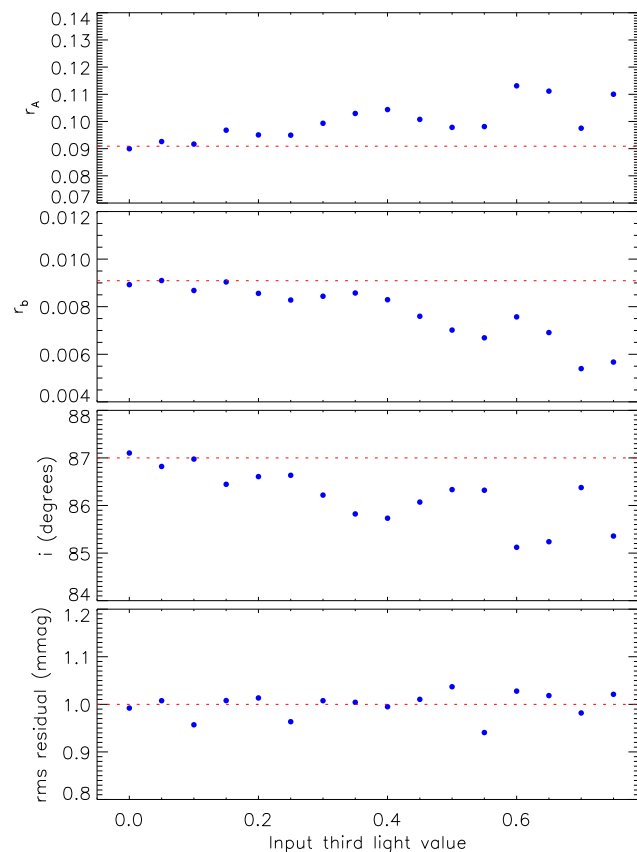

Figure 1. Plot of the variation of parameters fitted to a set of synthetic transit light curves with 1 mmag of Gaussian noise added. The synthetic datasets were generated for a range of third light values but fitted with the assumption of $L_3 = 0$. Dotted lines show the input parameter values for the synthetic light curve calculations.

2.4.1 The effect of third light

I have explored the possibility of measuring contaminating light by simulating a set of light curves with reasonable parameters ($r_A + r_b = 0.1$, $k = 0.1$, $i = 87°$). I added contaminating light (by convention referred to as 'third light' and expressed as a fraction of the total system light) by amounts ranging from $L_3 = 0$ to 0.75 in steps of 0.05. These were transformed into typical good ground-based light curves by retaining approximately 400 points within each transit and adding a Gaussian scatter with standard deviation 1 mmag. These synthetic light curves were then fitted with JKTEBOP under the assumption that $L_3 = 0$. The results (Fig. 1) show that the presence of L_3 results in systematic overestimates of r_A and underestimates of r_b and i. The bottom panel of Fig. 1 shows that the quality of the fit does *not* get worse as L_3 increases. Unaccounted third light therefore biases the resulting parameters without being detectable through its impact on the quality of the fit.

As a second test I modelled the same synthetic light curves again, this time fitting for third light. The resulting values of L_3 are shown in Fig. 2 and are extremely scattered as well as biased to smaller values. JKTEBOP deliberately does not restrict photometric parameters to physically realistic values (e.g. $L_3 \geqslant 0$), to avoid statistical biases in the uncertainties arising from Monte Carlo simulations. Fig. 2 demonstrates that there *is* a very small amount of information on L_3 in a good ground-based light curve, but that this
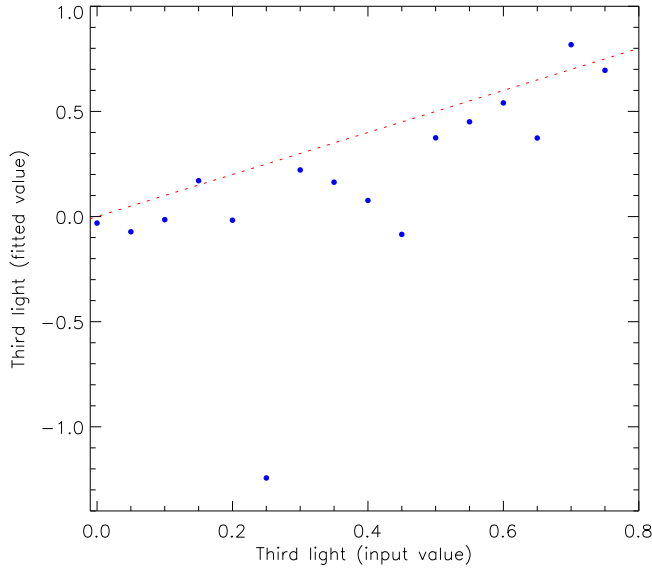
Figure 2. Plot of fitted versus input values of third light for the same light curves as in Fig. 1, but with L_3 included as a fitted parameter. The dotted line shows parity. Note the large scale on the y-axis.

Figure 3. Plot of the variation of parameters fitted to the same light curves as in Fig. 1, but in this case with L_3 included as a fitted parameter. The dotted lines show parity.

information is far too sparse to be useful. Fig. 3 shows the resulting values of the other main parameters: r_b and i are biased towards lower values and there is no trend visible in the sizes of the residuals.

In reality a large value of L_3 is not expected because such a bright star would show up in the spectroscopic observations of a transiting system. Fainter stars can be found via high-resolution imaging if they are slightly away from the planet host star (Daemgen et al. 2009). But it may never be possible to rule out the presence of a much fainter star ($L_3 < 5\%$ depending on the quality of the spectroscopic observations) which almost exactly co-incide with the planet host. As a guide, 5% of third light can be compensated for by increasing r_A by 1%, and decreasing r_b by 2% and i by 0.1°. It can therefore change the derived radius of the planet by several percent.

2.4.2 Accounting for third light

The observations of Daemgen et al. (2009) make it possible to account for third light when analysing transit light curves. They measured magnitude differences (light ratios) in the SDSS i and z passbands. When necessary I have propagated the light ratios to other passbands by convolving synthetic spectra from ATLAS9 model atmospheres (Kurucz 1979, 1993) with passband response functions made available by the Isaac Newton Group[6].

Armed with L_3 values for the correct passbands, I have included these in the same way as e and ω. JKTEBOP was modified to accept measured L_3 values as observations, and L_3 was included as a fitted parameter. Note that several published studies have instead simply subtracted L_3 from a light curve before analysis, which is statistically incorrect as it neglects the uncertainty in L_3.

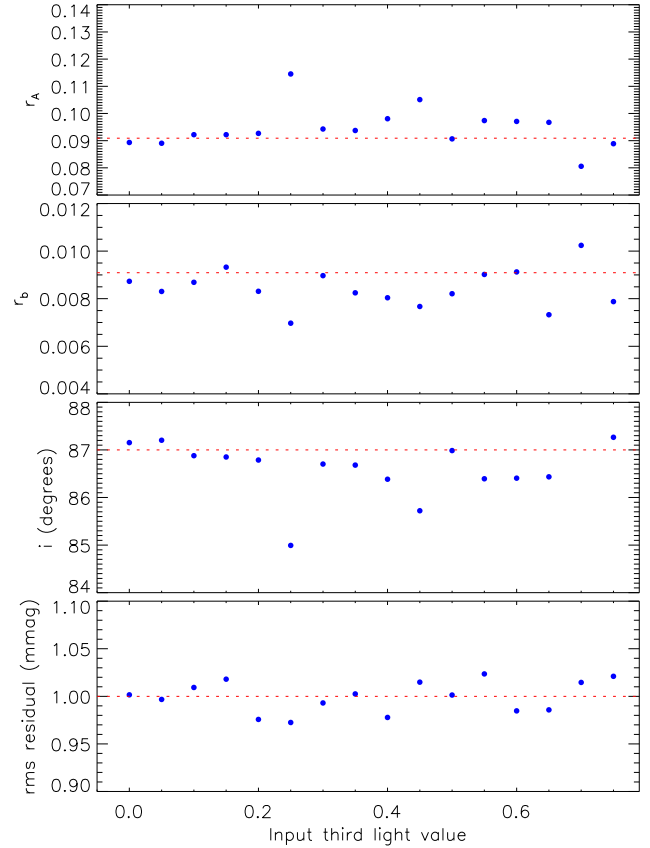Daemgen et al. (2009) surveyed fourteen transiting systems and detected faint companions to three of them. The companions are within 0.7–1.6″ of the transit host stars, and are fainter by generally 4 mag in the i band. Daemgen et al. found that their presence changed the physical properties of the TEPs by roughly 1σ. Of the three affected objects, TrES-2 and TrES-4 are analysed in the current work and WASP-2 is the subject of a separate publication (Southworth et al. 2010).

3 INCORPORATING STELLAR MODELS: ABSDIM

Analysis of a transit light curve gives the quantities r_A, r_b and i [7]. From RV measurements of the parent star it is possible to obtain e, ω, and the velocity amplitude of the star, K_A. With these observables we remain unfortunately one piece of information short of being able to calculate the full physical properties of the system. An additional constraint is needed, and this is generally supplied by forcing the properties of the star to match the predictions of theoretical stellar evolutionary models. To guide this process we can use the spectroscopically measured $T_{\rm eff}$ and metal abundance, $\left[\frac{\rm Fe}{\rm H}\right]$, of the star.

In the current work I adopt the method outlined in Paper II, in which the variable governing the solution process is taken to be K_b, the orbital velocity amplitude of the *planet*. An initial value of K_b

---

[6] http://catserver.ing.iac.es/filter/

[7] From transit light curves we also get $P_{\rm orb}$ and T_0. The uncertainty in $P_{\rm orb}$ is generally negligible, and T_0 does not enter the ABSDIM analysis.

Table 1. Physical ingredients and coverage of the stellar models used in this work. $Y_{\rm ini}$ is the primordial helium abundance, $\Delta Y/\Delta Z$ is the helium-to-metals enrichment ratio, $Z_{\odot}$ is the solar metal abundance (fraction by mass) and $\alpha_{\rm MLT}$ is the mixing length parameter.

Model set	Reference	Range in mass ($\rm M_{\odot}$)	Range in metal abundance (Z)	$Y_{\rm ini}$	$\dfrac{\Delta Y}{\Delta Z}$	$Z_{\odot}$	$\alpha_{\rm MLT}$	Notes
Claret	Claret (2004b, 2005, 2006, 2007)	0.2 to 1.5	0.01 to 0.05	0.24	2.0	0.02	1.68	Calculated on request
Y^2	Demarque et al. (2004)	0.4 to 5.2	0.00001 to 0.08	0.23	2.0	0.02	1.743	
Teramo	Pietrinferni et al. (2004)	0.5 to 10.0	0.0001 to 0.04	0.245	~1.4	0.0198	1.913	
VRSS	VandenBerg et al. (2006)	0.4 to 4.0	0.005 to 0.050	0.23544	2.2	0.188	1.90	
DSEP	Dotter et al. (2008)	0.1 to 5.0	0.000041 to 0.0404	0.245	1.6	0.0189	1.938	

is defined, usually in the region of $150\,{\rm km\,s^{-1}}$, and the full physical properties of the system are calculated using standard formulae (e.g. Hilditch 2001). Armed with the resulting stellar mass, $M_{\rm A}$, and $\left[\frac{\rm Fe}{\rm H}\right]$, I linearly interpolate within tabulated theoretical model results to find the predicted radius and $T_{\rm eff}$ of the star. This process is iteratively repeated whilst varying $K_{\rm b}$ in order to minimise the figure of merit

$$\mathrm{fom} = \left(\frac{r_{\rm A}^{\rm (obs)} - (R_{\rm A}^{\rm (pred)}/a)}{\sigma(\mathrm{r}_{\rm A}^{\rm (obs)})}\right)^2 + \left(\frac{T_{\rm eff}^{\rm (obs)} - T_{\rm eff}^{\rm (pred)}}{\sigma(T_{\rm eff}^{\rm (obs)})}\right)^2 \quad (3)$$

which results in the best-fitting system properties. In principle it is possible to also solve for the age of the system, but in practise the wide variety of evolutionary timescales of stars make this difficult. I therefore step through the possible ages of the star in 0.1 Gyr increments, starting at zero age and finishing when the star leaves the main sequence, in order to find the best overall solution. I do not make any attempt to match spectroscopically measured $\log g$ values as they are usually much less reliable than the surface gravity of the star calculated from the $M_{\rm A}$ and $R_{\rm A}$ obtained above. The above procedure implicitly applies the strong constraint on stellar density obtained from the light curve analysis (Seager & Mallén-Ornelas 2003).

The uncertainties in the system properties are calculated by a perturbation analysis, in which each input parameter is modified by its 1σ uncertainty and new solutions specified. The uncertainty for each output parameter is then calculated by adding the uncertainties due to each input parameter in quadrature. This perturbation analysis has the advantage of yielding detailed error budgets, where the effect of the uncertainty of every input parameter on every output parameter is specified. These error budgets indicate what additional observations are the best for improving our understanding of a specific TEP.

3.1 Which stellar models to use?

As outlined above, the physical properties of TEPs are calculated by forcing the properties of the parent star to match theoretical expectations. This dependence on theoretical predictions is a concern and will cause a systematic error. It is well known that whilst theoretical models are pretty good at reproducing the actual properties of stars, the various model sets are not flawless and do not agree perfectly with each other.

The existence of different theoretical model sets for low-mass stars opens the possibility of using several of them and explicitly deducing the systematic errors in TEP properties caused by their use. In Paper II six different sets of theoretical models were investigated and three adopted for calculating the planet properties. The *Siess* and *Cambridge-2007* models were in relatively poor agreement with other models, and the *Cambridge-2000* models had a lower coverage of the relevant parameter space than other models. I was therefore left with only three different model sets, which was insufficient to define high-quality systematic error estimates. On top of this, the *Padova* models included heavy element abundances only up to $Z = 0.03$ so did not cover quite a few transiting systems.

In the current paper I have therefore adopted the same solution procedure as introduced in Paper II, but with a significantly revised database of theoretical model predictions and with one more change. Instead of using the *Claret* models to define my baseline solutions and two other model sets to obtain systematic error estimates, I have used the unweighted mean and standard deviation of the results from all five model sets to describe the baseline solutions and systematic errors. The dependence of the final results on a single model set is therefore broken: all five model sets are treated equally and the choice of which sets of models to use becomes less important.

Of the sets of theoretical models included in Paper II, only the Y^2 models survive unchanged here (see Table 1). The *Claret* models have been supplemented by additional calculations for higher metal abundances of $Z = 0.06$ and 0.07. The third model set used here is *Teramo*[8] (Pietrinferni et al. 2004), and I selected the ones with moderate convective core overshooting (for masses $>1.1\,{\rm M_{\odot}}$), the standard mass loss law ($\eta = 0.4$) and normal elemental abundances (scaled-solar, i.e. no enhancement of the α-elements). For the fourth model set I acquired the Victoria-Regina (*VRSS*) models[9] (VandenBerg et al. 2006) with scaled-solar elemental abundances. In these models the convective core overshooting parameter depends on mass and is empirically calibrated. The fifth and final model set (*DSEP*) comes from Dartmouth Stellar Evolution Database[10] and again comprises the calculations with scaled-solar elemental abundances. I selected those models which follow the standard helium-to-metal enrichment law. The *DSEP* models include a contraction to the zero-age main sequence which can take tens of Myr.

In Fig. 4 I compare the predictions in mass and radius of the five sets of stellar models, for an age of 0.5 Gyr and for the adopted solar chemical composition (which differs between models). The models have a fairly good agreement in the mass–radius plane, particularly near $1.0\,{\rm M_{\odot}}$ as they are calibrated on the Sun, but a wider variety in the mass–$T_{\rm eff}$ plane. Also shown in Fig. 4 are the masses, radii and $T_{\rm eff}$ values of the sample of detached eclipsing binary star

---

[8] Obtained from the BaSTI database on 17/11/2009: http://albione.oa-teramo.inaf.it/
[9] Obtained on 18/11/2009 from http://www.cadc-ccda.hia-iha.nrc-cnrc.gc.ca/cvo/community/VictoriaReginaModels/.
[10] Obtained on 18/11/2009 from http://stellar.dartmouth.edu/~models/index.html.
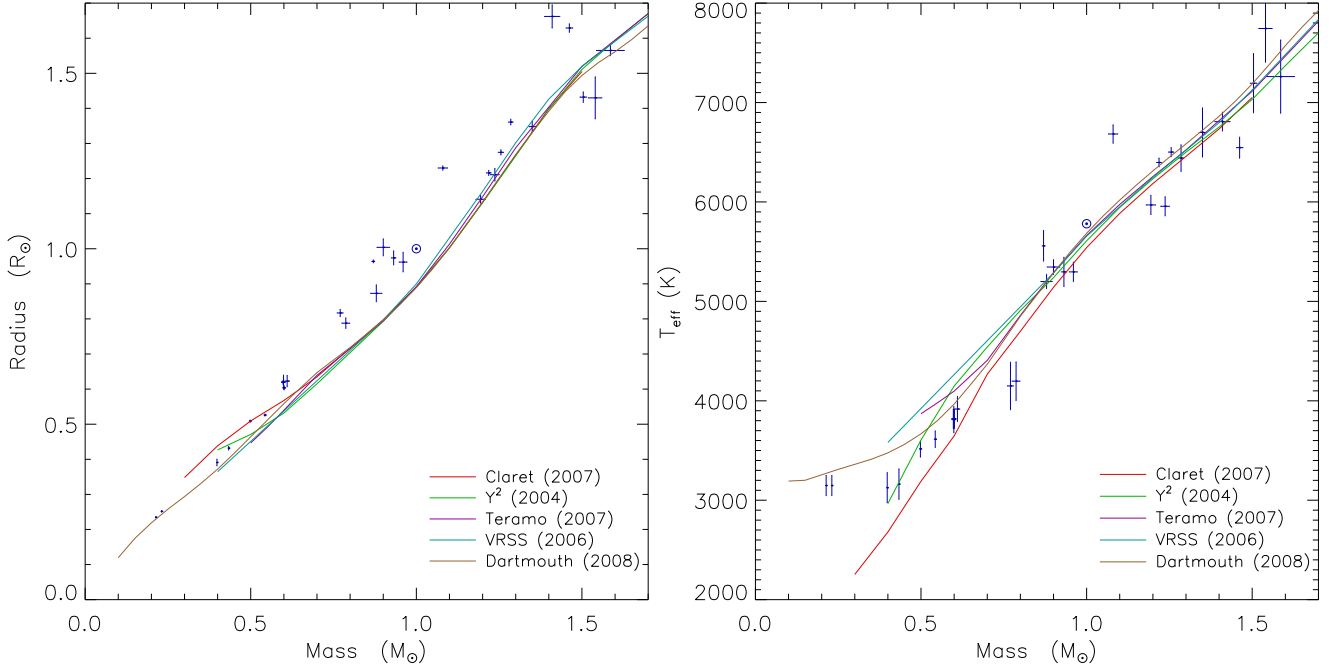
Figure 4. Mass–radius (left) and mass–$T_{\rm eff}$ (right) plots showing the predictions of the five sets of stellar models adopted in this work (solid lines). The predictions are for an age of 0.5 Gyr (to minimise the effects of evolution to and from the ZAMS) and for the solar chemical composition (which varies between models). The measured masses, radii and $T_{\rm eff}$ values of a sample of detached eclipsing binaries (see Paper II) are shown for comparison, using blue errorbars. The Sun is indicated by the usual $\odot$; note that the predictions of the models do not pass through the solar values on these plots as the Sun is much older than 0.5 Gyr.

systems constructed in Paper II. It can be seen that the disagreement with the models is much larger than the errorbars. This conclusion holds for all chemical compositions for which the five sets of models are available. Similarly, adopting an age either before or beyond the main sequence can provide an agreement for individual eclipsing binaries, but not for all of them simultaneously.

Fig. 4 illustrates what can be expected for the variation of systematic errors with mass. The models agree with each other very well in some regions, so systematics will be minimised, and less well at lower and higher masses, when systematics will be larger. The agreement between models is clearly much better than with the properties of well-studied eclipsing binaries. This means that using the five model sets will lead to only a *lower limit* on the systematic errors in the properties of TEPs. A probable upper limit to the systematic effects can be obtained by calculating solutions with an eclipsing binary mass–radius relation instead of a stellar model set; this is applied below and discussed further in Paper II.

3.2   Calculating the physical properties of transiting planets

Using the method and theoretical stellar models outlined above, the mass, radius, surface gravity and mean density of the star ($M_{\rm A}$, $R_{\rm A}$, $\log g_{\rm A}$, $\rho_{\rm A}$) and of the planet ($M_{\rm b}$, $R_{\rm b}$, $g_{\rm b}$, $\rho_{\rm b}$) can be calculated. For each TEP I have obtained results for each of the five stellar model sets and also using an empirical mass–radius relation defined by the eclipsing binaries. The final result for each parameter is the unweighted mean of the five stellar-model results. The statistical errorbar is taken to be the largest one from these five solutions and the systematic errorbar is taken to be the standard deviation of the parameter values from the five solutions. I include the final $K_{\rm b}$ value when possible to aid the comparison between different solu-

tions for the same planet. $K_{\rm b}$ is the parameter through which all of the stellar model dependence enters.

The surface gravity of the planet, $g_{\rm b}$, can be calculated from purely geometrical observed quantities (Southworth et al. 2007b) so has no systematic error. Similarly, the stellar density, $\rho_{\rm A}$, is independent of the stellar models (Seager & Mallén-Ornelas 2003) if $M_{\rm A} \gg M_{\rm b}$ is assumed.

In addition to the above parameters, I have also calculated the equilibrium temperature ($T_{\rm eq}$) and Safronov (1972) number (Θ) of the planet. $T_{\rm eq}$ is given by the equation

$$T_{\rm eq} = T_{\rm eff} \left(\frac{1-A}{4F} \right)^{1/4} \left(\frac{R_{\rm A}}{2a} \right)^{1/2} \tag{4}$$

where A is the Bond albedo and F is a heat redistribution factor. Because A and F are not known precisely I instead calculate a modified equilibrium temperature ($T'_{\rm eq}$) which equals $T_{\rm eq}$ if $A = 1 - 4F$:

$$T'_{\rm eq} = T_{\rm eff} \left(\frac{R_{\rm A}}{2a} \right)^{1/2} = T_{\rm eff} \left(\frac{r_{\rm A}}{2} \right)^{1/2} \tag{5}$$

The Safronov number is defined as the ratio of the escape velocity to the orbital velocity of the planet:

$$\Theta = \frac{1}{2} \left(\frac{V_{\rm esc}}{V_{\rm orb}} \right)^2 = \left(\frac{a}{R_{\rm b}} \right) \left(\frac{M_{\rm b}}{M_{\rm A}} \right) = \frac{1}{r_{\rm b}} \frac{M_{\rm b}}{M_{\rm A}} \tag{6}$$

From Eq. 5 above it can be seen that $T'_{\rm eq}$ depends only on the stellar $T_{\rm eff}$ and the fractional radius obtained from the light curve analysis. $T'_{\rm eq}$ therefore turns out (like $g_{\rm b}$) to be independent of the stellar models, but does have some systematic error as it is dependent on the effective temperature scale of low-mass (F, G and K) stars.

Table 2. Parameters from the light curve analyses presented here and in previous works, and used here to determine the physical properties of the TEPs. The orbital periods are taken from the literature, and the bracketed numbers represent the uncertainty in the preceding digits. Systems for which orbital eccentricity was accounted for are indicated with a $\star$ in the column marked "e?".

System	Orbital period (days)	e?	Orbital inclination, i (degrees)	Fractional stellar radius, r_A	Fractional planetary radius, r_b	Reference
GJ 436	2.64389524 (76)	$\star$	86.43 ± 0.18	0.0731 ± 0.0027	0.00605 ± 0.00023	Paper I
HAT-P-1	4.4652934 (93)		86.25 ± 0.22	0.0935 ± 0.0025	0.01051 ± 0.00031	This work
HAT-P-2	5.6334729 (61)	$\star$	85.9 ± 1.5	0.1247 ± 0.0106	0.00847 ± 0.00082	This work
HD 149026	2.8758911 (25)		88.0 ± 2.0	$0.140^{+0.012}_{-0.006}$	$0.0068^{+0.0011}_{-0.0008}$	Paper I
HD 189733	2.21857578 (80)		85.78 ± 0.25	0.1113 ± 0.0031	0.0175 ± 0.0005	Paper I
HD 209458	3.52474859 (38)		86.590 ± 0.046	0.11384 ± 0.00041	0.01389 ± 0.00006	Paper I
OGLE-TR-10	3.101278 (4)		83.87 ± 0.69	0.157 ± 0.009	0.0182 ± 0.0011	Paper I
OGLE-TR-56	1.211909 (1)		79.8 ± 2.4	0.245 ± 0.026	0.0241 ± 0.0034	Paper I
OGLE-TR-111	4.0144479 (41)		88.11 ± 0.66	0.0842 ± 0.0038	0.01107 ± 0.00067	Paper I
OGLE-TR-113	1.4324757 (13)		87.7 ± 1.4	0.1592 ± 0.0043	0.02331 ± 0.00089	This work
OGLE-TR-132	1.689868 (3)		83.3 ± 2.4	0.211 ± 0.020	0.0198 ± 0.0024	Paper I
OGLE-TR-182	3.97910 (1)		84.3 ± 1.2	0.137 ± 0.014	0.0135 ± 0.0013	This work
OGLE-TR-211	3.67724 (3)		88.0 ± 2.0	$0.1422^{+0.0150}_{-0.0083}$	$0.01181^{+0.00146}_{-0.00083}$	This work
OGLE-TR-L9	2.485533 (7)		82.07 ± 0.69	0.1731 ± 0.0083	0.01910 ± 0.00085	This work
TrES-1	3.0300728 (6)		88.67 ± 0.71	0.0964 ± 0.0018	0.01331 ± 0.00035	Paper I
TrES-2	2.4706101 (18)		83.80 ± 0.36	0.1282 ± 0.0035	0.01658 ± 0.00043	This work
TrES-3	1.3061864 (5)		82.07 ± 0.17	$0.1666^{+0.0017}_{-0.0015}$	$0.02731^{+0.00055}_{-0.00043}$	This work
TrES-4	3.553945 (75)		81.53 ± 0.60	0.1802 ± 0.0083	0.0174 ± 0.0012	This work
WASP-1	2.519961 (18)		88.0 ± 2.0	$0.1737^{+0.0057}_{-0.0089}$	$0.0182^{+0.0007}_{-0.0011}$	Paper I
WASP-2	2.15222144 (39)		84.81 ± 0.17	0.1238 ± 0.0018	0.01643 ± 0.00030	Southworth et al. (2010)
WASP-3	1.846835 (2)		84.1 ± 1.3	0.201 ± 0.010	0.0218 ± 0.0011	This work
WASP-4	1.33823150 (61)		89.0 ± 1.0	$0.1825^{+0.0011}_{-0.0010}$	$0.02812^{+0.00022}_{-0.00014}$	Southworth et al. (2009b)
WASP-5	1.6284246 (13)		85.8 ± 1.1	0.1847 ± 0.0061	0.02050 ± 0.00091	Southworth et al. (2009a)
WASP-10	3.0927616 (10)	$\star$	88.81 ± 0.40	0.0865 ± 0.0041	0.01349 ± 0.00065	This work
WASP-18	0.94145181 (44)	$\star$	85.0 ± 2.1	0.2795 ± 0.0084	0.0272 ± 0.0012	Southworth et al. (2009c)
XO-1	3.9415128 (28)		89.06 ± 0.84	0.0886 ± 0.0019	0.01166 ± 0.00035	Paper I
XO-2	2.6158640 (16)		88.8 ± 1.2	$0.1237^{+0.0024}_{-0.0047}$	$0.01300^{+0.00033}_{-0.00070}$	This work
XO-3	3.1915289 (32)	$\star$	83.89 ± 0.40	0.1447 ± 0.0046	0.01317 ± 0.00047	This work
XO-4	4.12502 (2)		$89.9^{+0.1}_{-3.9}$	$0.1300^{+0.0283}_{-0.0051}$	$0.01124^{+0.00334}_{-0.00054}$	This work
XO-5	4.187757 (11)		87.04 ± 0.65	0.1004 ± 0.0049	0.01054 ± 0.00073	This work

4 RESULTS FOR INDIVIDUAL SYSTEMS

In this section I present the photometric (JKTEBOP) and absolute-dimensions (ABSDIM) analyses of a set of thirty TEPs based on high-quality data. In many cases I adopt the JKTEBOP results from Paper I or later works (Southworth et al. 2009a,b,c, 2010). The final JKTEBOP results of all TEPs are collected in Table 2, which also includes the orbital periods and indicates for which systems a non-circular orbit was adopted. The mass ratio of each TEP is required as an input parameter for the light curve analysis, but in all cases its effect on the solution is negligible. Representative values have been taken from the literature but will not be discussed further.

The physical properties of all thirty TEPs are obtained or revised in the current work, using the new theoretical model sets discussed in Sect. 3. This also requires $T_{\rm eff}$, $\left[\frac{\rm Fe}{\rm H}\right]$ and K_A values for each system. These are summarised in Table 3. The values are mostly unchanged for the fourteen TEPs studied in Paper II, but in a few cases improved values have become available and replace the previous entries. In Papers I and II the individual systems were tackled roughly in order of increasing complexity. The current work reverts to the more structured approach of attacking the TEPs in alphabetical order, beginning with those objects for which a light curve analysis is presented (Sects. 4.1 to 4.15, then moving on to those whose photometric parameters are adopted unchanged from Paper I (Sect. 4.16).

4.1 HAT-P-1

HAT-P-1 was found to be a TEP by Bakos et al. (2007a) from data taken by the HAT survey (Bakos et al. 2002, 2004). Its low mass $(0.5\,{\rm M_{Jup}})$ and large radius $(1.2\,{\rm R_{Jup}})$ make it one of the least dense exoplanets known. Excellent light curves from the FLWO 1.2 m (z band), Lick 1.0 m Nickel (Z band) and Wise 1.0 m telescopes were presented by Winn et al. (2007c) and the first two of these were included in Paper I. Since then additional data from the Nickel (Z band) and the Hawaiian 2 m Magnum (V band) telescopes have been obtained by Johnson et al. (2008). In this work I have analysed the latter two datasets in order to refine the results from Paper I. In both cases I have adopted solutions with the linear LD coefficient fitted and the nonlinear coefficient fixed but perturbed in the Monte Carlo simulations ('LD fit/fix'). The residual permutation analyses indicate that correlated errors are important for both datasets.

The final light curve parameters are the weighted means of those for the four studied datasets. The results agree well with each other except for k, for which $\chi_\nu^2 = 2.8$. The errorbar for k has been multiplied by $\sqrt{2.8}$ to account for this. The light curve fits are plotted in Fig. 5 and summarised in Table A3. They are in good agreement with literature values.

The physical properties of HAT-P-1 have been calculated using the five different sets of stellar evolutionary models plus the

Table 3. Measured quantities for the parent stars which were adopted in the analysis presented in this work.

System	Velocity amplitude (m s^{-1})		$T_{\rm eff}$ (K)	Reference	$\left[\frac{\rm Fe}{\rm H}\right]$	Reference
GJ 436	18.34 ± 0.52	Maness et al. (2007)	3500 ± 100	Bean et al. (2006)	-0.03 ± 0.2	Bonfils et al. (2005)
HAT-P-1	59.3 ± 1.4	Johnson et al. (2008)	5975 ± 50	Bakos et al. (2007a)	0.13 ± 0.05	Bakos et al. (2007a)
HAT-P-2	983.9 ± 17.2	Pál et al. (2010)	6290 ± 60	Pál et al. (2010)	0.14 ± 0.08	Pál et al. (2010)
HD 149026	43.3 ± 1.2	Sato et al. (2005)	6147 ± 50	Sato et al. (2005)	0.36 ± 0.05	Sato et al. (2005)
HD 189733	200.56 ± 0.88	Boisse et al. (2009)	5050 ± 50	Bouchy et al. (2005b)	-0.03 ± 0.05	Bouchy et al. (2005b)
HD 209458	85.1 ± 1.0	Naef et al. (2004)	6117 ± 50	Santos et al. (2004)	0.02 ± 0.05	Santos et al. (2004)
OGLE-TR-10	80 ± 17	Konacki et al. (2005)	6075 ± 86	Santos et al. (2006)	0.28 ± 0.10	Santos et al. (2006)
OGLE-TR-56	212 ± 22	Bouchy et al. (2005a)	6119 ± 62	Santos et al. (2006)	0.25 ± 0.08	Santos et al. (2006)
OGLE-TR-111	78 ± 14	Pont et al. (2004)	5044 ± 83	Santos et al. (2006)	0.19 ± 0.07	Santos et al. (2006)
OGLE-TR-113	267 ± 34	TWH08	4804 ± 106	Santos et al. (2006)	0.15 ± 0.10	Santos et al. (2006)
OGLE-TR-132	167 ± 18	Moutou et al. (2004)	6210 ± 59	Gillon et al. (2007)	0.37 ± 0.07	Gillon et al. (2007)
OGLE-TR-182	120 ± 17	Pont et al. (2008)	5924 ± 64	Pont et al. (2008)	0.37 ± 0.08	Pont et al. (2008)
OGLE-TR-211	82 ± 16	Udalski et al. (2008)	6325 ± 91	Udalski et al. (2008)	0.11 ± 0.10	Udalski et al. (2008)
OGLE-TR-L9	510 ± 170	Snellen et al. (2009)	6933 ± 58	Snellen et al. (2009)	-0.05 ± 0.20	Snellen et al. (2009)
TrES-1	115.2 ± 6.2	Alonso et al. (2004)	5226 ± 50	Santos et al. (2006)	0.06 ± 0.05	Santos et al. (2006)
TrES-2	181.3 ± 2.6	O'Donovan et al. (2006)	5795 ± 73	Ammler-von Eiff et al. (2009)	0.06 ± 0.08	Ammler-von Eiff et al. (2009)
TrES-3	369 ± 11	Sozzetti et al. (2009)	5650 ± 75	Sozzetti et al. (2009)	-0.19 ± 0.08	Sozzetti et al. (2009)
TrES-4	97.4 ± 7.2	Mandushev et al. (2007)	6200 ± 75	Sozzetti et al. (2009)	0.14 ± 0.09	Sozzetti et al. (2009)
WASP-1	111 ± 9	Wheatley et al. (2010)	6110 ± 50	Stempels et al. (2007)	0.23 ± 0.08	Stempels et al. (2007)
WASP-2	153.6 ± 3.0	Triaud et al. (2010)	5150 ± 80	Triaud et al. (2010)	-0.08 ± 0.08	Triaud et al. (2010)
WASP-3	290.5 ± 9.5	Tripathi et al. (2010)	6400 ± 100	Pollacco et al. (2008)	0.00 ± 0.20	Pollacco et al. (2008)
WASP-4	$242.1^{+2.8}_{-3.1}$	Triaud et al. (2010)	5500 ± 100	Gillon et al. (2009)	-0.03 ± 0.09	Gillon et al. (2009)
WASP-5	268.7 ± 1.8	Triaud et al. (2010)	5700 ± 100	Gillon et al. (2009)	0.09 ± 0.09	Gillon et al. (2009)
WASP-10	553.1 ± 7.5	Johnson et al. (2009b)	4675 ± 100	Christian et al. (2009)	0.03 ± 0.20	Christian et al. (2009)
WASP-18	1816.9 ± 2.0	Triaud et al. (2010)	6400 ± 100	Hellier et al. (2009)	0.00 ± 0.09	Hellier et al. (2009)
XO-1	116.0 ± 9.0	McCullough et al. (2006)	5750 ± 50	McCullough et al. (2006)	0.02 ± 0.05	McCullough et al. (2006)
XO-2	85 ± 8	Burke et al. (2007)	5340 ± 50	Burke et al. (2007)	0.45 ± 0.05	Burke et al. (2007)
XO-3	1488 ± 10	Winn et al. (2009)	6429 ± 75	Johns-Krull et al. (2008)	-0.18 ± 0.05	Johns-Krull et al. (2008)
XO-4	163 ± 16	McCullough et al. (2008)	6397 ± 70	McCullough et al. (2008)	-0.04 ± 0.05	McCullough et al. (2008)
XO-5	144.9 ± 2.0	Pál et al. (2009)	5370 ± 70	Pál et al. (2009)	0.05 ± 0.06	Pál et al. (2009)

empirical mass–radius relation from Paper II. The individual solutions are given in Table A4 and then compared with literature values, where a good agreement is found.

4.2 HAT-P-2

HAT-P-2 was discovered to be a TEP system by Bakos et al. (2007b), under the name HD 147506. It is a very bright system ($V = 8.7$) with a massive planet ($M_{\rm b} = 8.74\,{\rm M_{Jup}}$) in a highly eccentric orbit. It has been found not to exhibit a spin–orbit misalignment (Winn et al. 2007a; Loeillet et al. 2008), in contrast to other massive TEPs on eccentric orbits (Johnson et al. 2009a).

Good z-band light curves of HAT-P-2 have been published by Bakos et al. (2007b), covering one transit with the FLWO 1.2 m, and by Pál et al. (2010), covering another six transits with the FLWO 1.2 m and the Perkins telescopes. Here I analyse the FLWO datasets together, omitting the small amount of data taken on the night of 2007/03/18, as well as the Perkins data. One complication is the orbital eccentricity: this was accounted for using the method discussed in Sect. 2.3 and adopting the constraints $e\cos\omega = -0.5152 \pm 0.0036$ and $e\sin\omega = -0.0441 \pm 0.0084$ (Pál et al. 2010). In both cases correlated errors were not important and the LD fit/fix solutions were adopted. The best fits are shown in Fig. 6.

The two light curve solutions unfortunately do not agree very well (9.3σ discrepancy in k). I therefore adopt the FLWO 1.2 m results, as these are the much more extensive of the two sets of data and have full coverage of the transit phases. The FLWO results

agree well with those of Pál et al. (2010), for which most of the data come from, but have a larger $r_{\rm A}$ and $r_{\rm b}$ than other literature values (Table A7).

As expected given the light curve results, my ABSDIM analysis returns system properties in good agreement with those of Pál et al. (2010) but not with other literature studies (Table A8). The prime mover in the most recent solutions is $r_{\rm A}$, which has a strong effect on the density of the star and thus the other physical properties. The radius of the planet is uncertain by 10%, despite the existence of a high-quality light curve for HAT-P-2, because the transit depth is shallow (0.6%). An improved photometric study is warranted.

4.3 OGLE-TR-113

Like OGLE-TR-132 (studied in Paper I), OGLE-TR-113 was identified as a possible planetary system by Udalski et al. (2002) and its nature was confirmed by Bouchy et al. (2004) using the OGLE light curve and new RV measurements. It was independently confirmed as a TEP by Konacki et al. (2004), also from the OGLE light curve and high-precision RVs, and an abundance analysis of the parent star has been presented by Santos et al. (2006). Whilst OGLE-TR-113 exhibits a deep transit, its photometric tractability is hindered by the presence of a brighter star only $3''$ away.

Apart from the OGLE discovery observations (Udalski et al. 2002), three photometric studies of OGLE-TR-113 have been published. Gillon et al. (2006) used the ESO New Technology Telescope (NTT) and SUSI2 imager to observe two transits in the R band, and obtained what is currently the best light curve of OGLE-
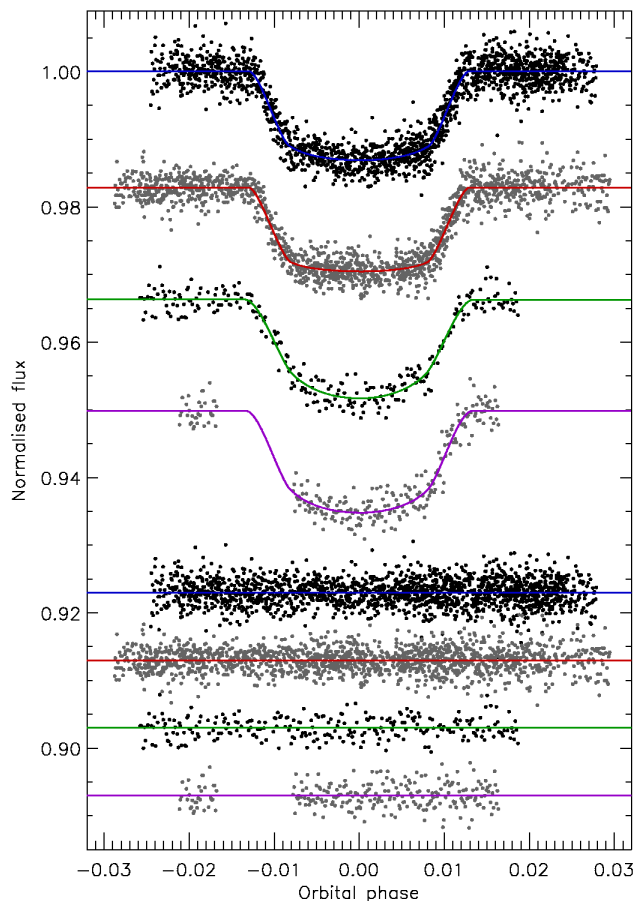
Figure 5. Phased light curves of HAT-P-1 compared to the best fits found using JKTEBOP and the quadratic LD law in Paper I and in this work. The best fits and residuals are offset from unity and zero fluxes, respectively, for display purposes. The light curves are, from top to bottom, FLWO z-band (Winn et al. 2007c), Lick Z-band (Winn et al. 2007c), Magnum V-band (Johnson et al. 2008) and Nickel Z-band (Johnson et al. 2008).

Figure 6. Phased z-band light curves of HAT-P-2 compared to the best fits found using JKTEBOP and the quadratic LD law. The best fits and residuals are offset for display purposes. The upper light curve is from the FLWO 1.2 m (Bakos et al. 2007b; Pál et al. 2010) and the lower is from the Perkins 1.8 m (Pál et al. 2010).

a few Gyr, and in several cases is up against the edge of the stellar model grid at 20 Gyr. Aside from that, the properties of the star and planet are rather well-determined but would benefit from an improved K_A value as well as a better light curve. The agreement with literature studies is good, although it seems that in some cases the published errorbars are smaller than one would expect.

4.4 OGLE-TR-182

OGLE-TR-182 is the sixth TEP discovered as a result of the OGLE search for light variability in selected fields in the Southern hemisphere. Its discovery and analysis was presented by Pont et al. (2008), which remains the only study of this object to date. OGLE-TR-182 is difficult because of its faintness ($V = 16.8$ and $I = 15.9$) and crowded field. Pont et al. (2008) obtained 24 RV measurements using VLT/FLAMES/UVES, and a light curve with VLT/FORS1.

The VLT light curve is analysed here and is rather affected by correlated noise. Including the linear LD coefficients as a fitted parameter gives substantially better fits than with both LD coefficients fixed, but the data cannot support the determination of both LD coefficients. I therefore adopt the LD fit/fix solutions (see Fig. 8 and Table A15), which are not in good agreement with Pont et al. (2008). Compared to these authors I find a solution with a lower i and a correspondingly larger star and planet.

The physical properties of OGLE-TR-182 are summarised in Table A16 and point to a planet with a rather low density of $0.33 \, \rho_{\rm Jup}$. However, my results are rather different to those of Pont et al. (2008), and are in poorer agreement with the measured spectroscopic $T_{\rm eff}$ and (rather uncertain) $\log g$ measurement. My analysis procedure is more sensitive to the quality of the light curve

TR-113. Snellen & Covino (2007) observed a K-band transit and an occultation of the system using NTT/SOFI, and detected the occultation with a significance of 2.8σ. Díaz et al. (2007) obtained V-band photometry of one transit using a Very Large Telescope (VLT) and the VIMOS instrument; additional data taken in the I and K_s bands are unavailable and of lower quality.

In this work I analyse the Gillon et al. observations, the Snellen & Covino transit light curve, and the V-band data obtained by Díaz et al. For the second of these three datasets I allowed for light from the planet with a surface brightness ratio of 0.07 ± 0.02. The surface brightness ratio is a parameter of the JKTEBOP model which is important for eclipsing binary systems but usually left at zero for transiting systems due to the faintness of the planet with respect to the star. The best fits are shown in Fig. 7 and given in Table A12. In all three cases correlated noise is not important. For the Snellen light curve I had to adopt solutions with both LD coefficients fixed, but for the other two I was able to use the LD fit/fix solutions. The final results for the Gillon and Snellen data are in good agreement. The solution of the Díaz data prefers a rather higher i and lower $r_{\rm A}$ and $r_{\rm b}$. I therefore combined the Gillon and Snellen data results to obtain the final light curve parameters.

The resulting physical properties of OGLE-TR-113 are given in Table A13. The system age is constrained only to be more than
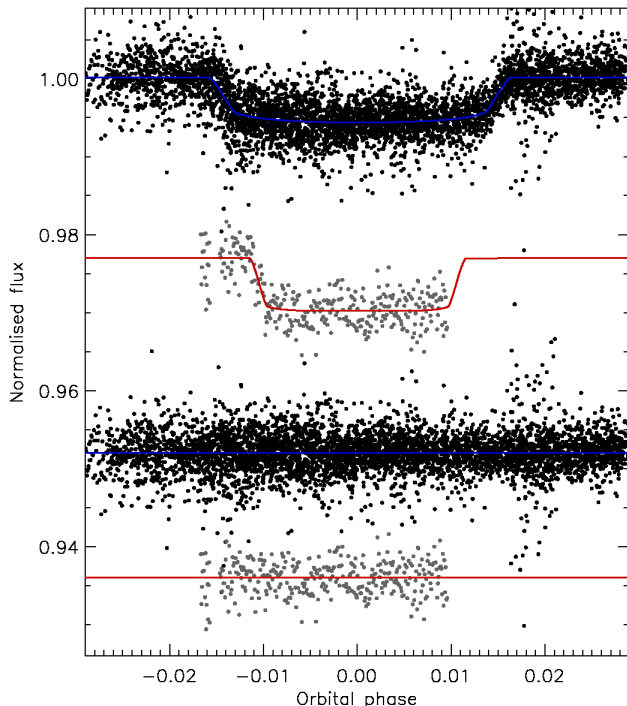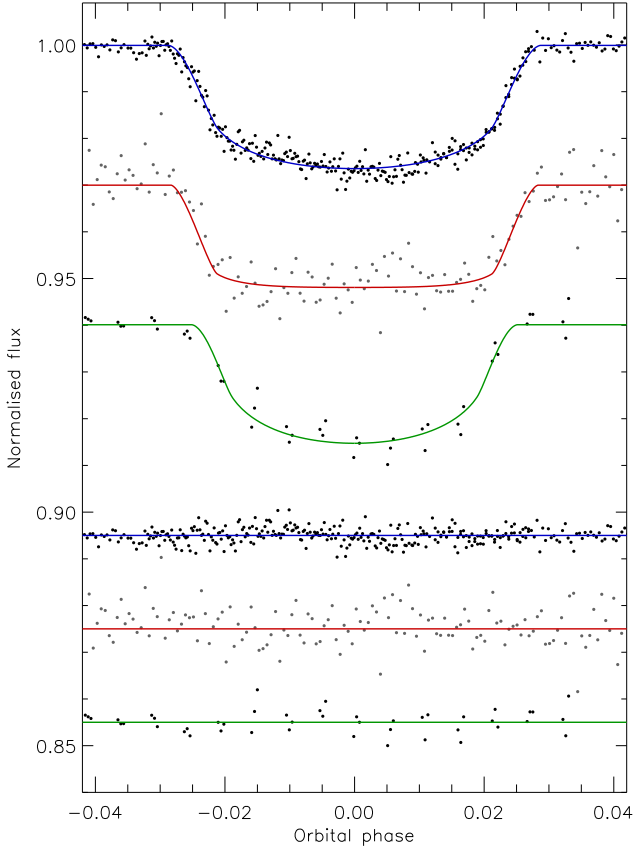
Figure 7. Phased light curves of OGLE-TR-113 with the best fits found using JKTEBOP and the quadratic LD law and residuals of the fits. From top to bottom the datasets are Gillon et al. (2006) (R-band), Snellen & Covino (2007) (K_s-band, binned by $\times 5$ for display purposes) and Díaz et al. (2007) (V-band).
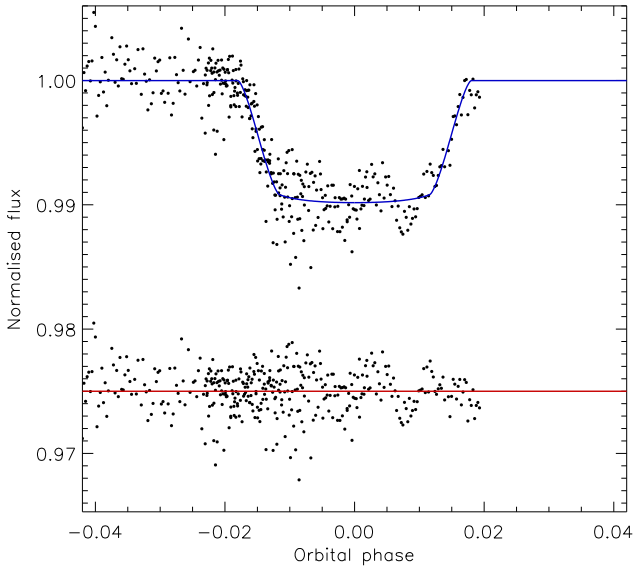

Figure 8. Phased VLT light curve of OGLE-TR-182 from Pont et al. (2008) compared to the best fit found using JKTEBOP and the quadratic LD law. The residuals are offset from zero for display purposes.

Figure 9. Phased VLT light curve of OGLE-TR-211 from Udalski et al. (2008) compared to the best fit found using JKTEBOP and the quadratic LD law. The residuals are offset from zero for display purposes.

than the more 'global' approach taken by Pont et al., so is potentially more susceptible to correlated noise. This possibility should be investigated by acquiring a new light curve, under good seeing conditions to cope with the crowded field.

4.5   OGLE-TR-211

OGLE-TR-211 is the seventh TEP discovered using OGLE data (Udalski et al. 2008). Its relative faintness means that the available follow-up photometry and spectroscopy is not definitive. The parent star is more massive and also more evolved than the Sun, which results in the transit being rather shallow (Fig. 9). Here I analyse the VLT light curve presented by Udalski et al. (2008), ignoring the observational errors supplied with the data which are quite discretised (the only values are 0.001, 0.002 and 0.003) and contribute to instability in the light curve solution.

I am not able to get a determinate solution to the VLT data. Possible fits occupy a locus extending from a high i with low r_A to a lower i with a large r_A. I have therefore calculated solutions for a range of i values and retained only those which in the ABSDIM analysis result in a T_{eff} within a conservative 3σ of the observed value. The observed stellar $\log g$ did not provide a useful constraint. Allowable solutions extend from $i = 90°$ down to a sharp cut-off around $i = 86.25°$ so I present solutions for $i = 86, 88,$ and $90°$ in Table A17. For the final result I accept the LD fit/fix solutions for $i = 88°$ but specify errors which account for both the Monte Carlo errorbars and the variation between the different solutions (Table A18). The correlated errors are again important, as can be seen in Fig. 9.

The physical properties of OGLE-TR-211 are shown in Table A19 and are in reasonable agreement with those of Udalski et al. (2008) except for the planetary mass. M_b depends mainly on the measured K_A, for which both studies have used the same value, so it is not clear why such a discrepancy should arise. Table A19 includes the first determinations of the age and density of the star, planetary equilibrium temperature (which is quite high at $T'_{\mathrm{eq}} = 1686^{+90}_{-55}$ K) and Safronov number. The system age is
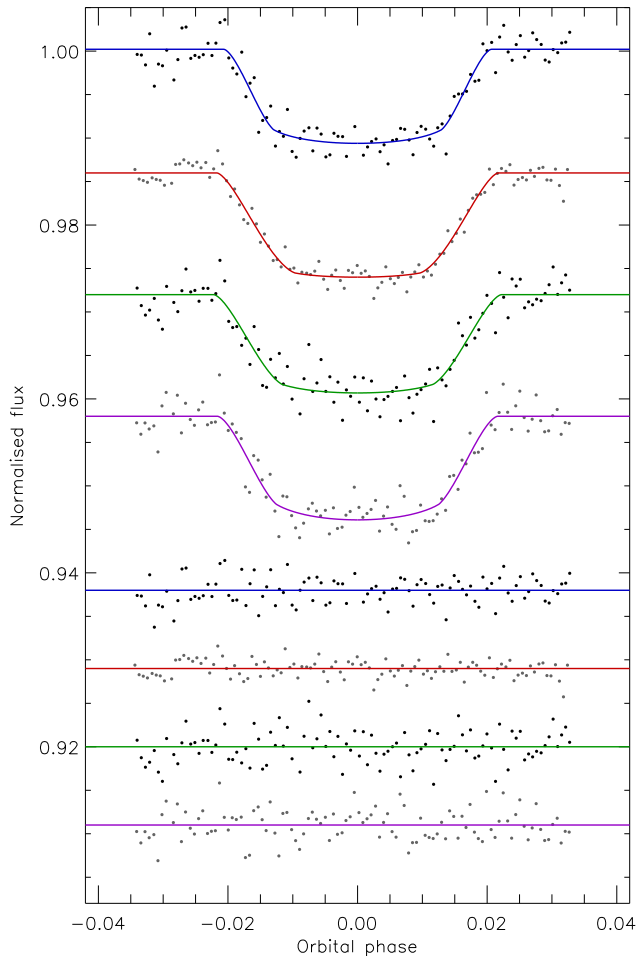
Figure 10. Phased GROND light curves of OGLE-TR-L9 from Snellen et al. (2009) compared to the best fit found using JKTEBOP and the quadratic LD law. From top to bottom the light curves are g, r, i and z. The residuals are offset from zero to the base of the figure.

relatively well determined ($2.6^{+0.6}_{-0.7}\,{}^{+0.4}_{-0.3}$ Gyr) because the star has evolved away from the zero-age main sequence. OGLE-TR-211 would certainly benefit from additional spectroscopic and photometric observations.

4.6 OGLE-TR-L9

OGLE-TR-L9 was discovered within the OGLE-II survey data (Udalski et al. 1997) by Snellen et al. (2009), and is a relatively massive planet orbiting a rapidly-rotating ($V_{\sin i} = 39\,\mathrm{km\,s^{-1}}$) F3 V star. High-quality follow-up light curves were obtained by Snellen et al. using the newly-commissioned GROND instrument (Greiner et al. 2008) on the 2.2 m telescope at ESO La Silla. GROND is a CCD imager which utilises dichroics to observe simultaneously in seven passbands (SDSS $griz$ and near-infrared JHK). In the case of OGLE-TR-L9 the JHK data were too noisy to be useful, but the $griz$ data are of good quality (Fig. 10).

The $griz$ observations have been analysed here (Tables A20 to A23). The gri light curves are good enough to support LD fit/fix solutions but for the z data both LD coefficients were held fixed. The parameters for the four light curves were combined to obtain the final photometric results (Table A24). Their agreement with those of Snellen et al. (2009) is not good – i and r_{A} are correlated and
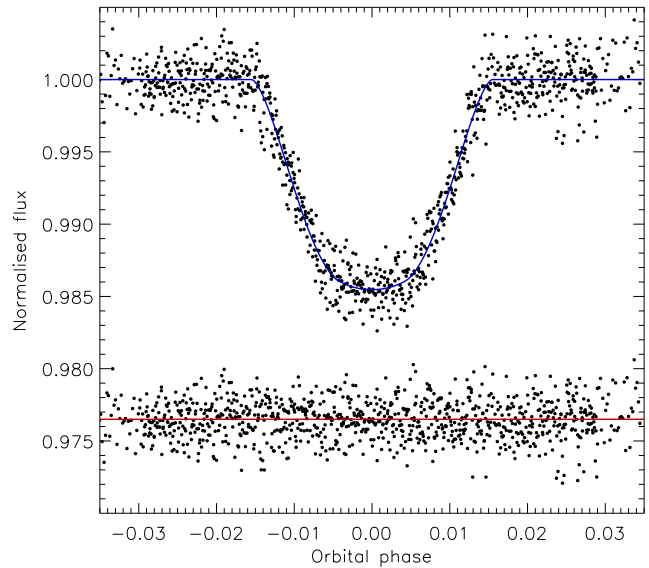

Figure 11. Phased light curve of the transits of TrES-2 from Holman et al. (2007) compared to the best fit found using JKTEBOP and the quadratic LD law with the linear LD coefficient included as a fitted parameter. The residuals of the fit are plotted at the bottom of the figure, offset from zero.

my solution corresponds to a significantly higher i (3σ) and lower r_{A} and r_{b} (both 6σ).

The ABSDIM results for OGLE-TR-L9 (Table A25) are in reasonable agreement with those of Snellen et al. (2009), which is surprising given the differences in the photometric parameters. One reason for this is that the ABSDIM solution is governed mainly by the observed T_{eff} (which has a relative uncertainty of 0.8%) rather than by r_{A} (5%). I find that OGLE-TR-L9 b has one of the highest T'_{eq}s (2039 ± 51 K) of any known TEP. Aside from its faintness, this planet is an excellent candidate for multicolour 'transmission photometry' to detect variations in planetary radius with wavelength due to atmospheric opacity effects (Fortney et al. 2008). The system would benefit from additional spectroscopy to provide improved measurements of $\left[\frac{\mathrm{Fe}}{\mathrm{H}}\right]$ and K_{A}. This subsection completes my analysis of the TEPs discovered from OGLE survey data.

4.7 TrES-2

TrES-2 was the second TEP discovered by the Trans-Atlantic Exoplanet Survey (O'Donovan et al. 2006) and is both larger and more massive than Jupiter. Excellent ground-based light curves of three transits were obtained and studied by Holman et al. (2007), in close collaboration with Sozzetti et al. (2007). The relatively low orbital inclination of this system ($i = 83.8°$) help r_{A} and r_{b} to be determined to a high accuracy.

The Holman z-band light curve of TrES-2 was studied in Paper I, but is revisited here because Daemgen et al. (2009) have since found a fainter star separated from TrES-2 by 1.089 ± 0.008 arcsec and with a magnitude difference of $\Delta z = 3.429 \pm 0.010$ (see Sect. 2.4).

TrES-2 is of additional interest because Mislis & Schmitt (2009) found a possible decrease in the transit duration between their own and Holman's observations. This would most likely indicate that the orbital inclination is getting lower, which in turn points to the presence of a low-mass third body in the TrES-2 system. Scuderi et al. (2009) obtained new data which did not confirm

this hypothesis, but Mislis et al. (2009) have since resurrected the changing i. In addition, Rabus et al. (2009) presented a transit timing study of TrES-2 which found a small sinusoidal perturbation with a 0.2 day period, but with only moderate statistical significance. TrES-2 is in the field of view of the NASA *Kepler* satellite (Koch et al. 2010), so a light curve of remarkable quality should become available for future investigations of these possibilities.

Here I reanalyse the z-band light curve of Holman et al. (2007), this time with the incorporation of a third light value of $L_3(z) = 0.0408 \pm 0.0004$. From the adopted $T_{\rm eff}$ of TrES-2 A (Table 3) and the magnitude differences in i and z (Daemgen et al. 2009) I find that the fainter companion star has $T_{\rm eff} = 4390 \pm 70$ K (consistent with the $\sim$K5 spectral type found by Daemgen et al. 2009), and is substantially further away than TrES-2 so is not physically bound to the system.

The results of the JKTEBOP analysis are given in Table A26 and I adopt the LD fit/fix results. Correlated noise is not important. Table A27 shows a comparison with the results from Paper I, in which the analysis did not account for the faint companion star: k has decreased by 1σ whilst $r_{\rm A} + r_{\rm b}$ and $r_{\rm A}$ become smaller by less than 0.5σ. The best fit is shown in Fig. 11.

The physical properties of the TrES-2 system are summarised in Table A28. My results agree with literature studies within the errors, although $M_{\rm A}$ and $M_{\rm b}$ are larger by roughly 1σ. This can be traced back to the slightly smaller $r_{\rm A}$ found above. More precise spectroscopic $T_{\rm eff}$ and $\left[\frac{\rm Fe}{\rm H}\right]$ values would allow improved system parameters to be obtained, as would better photometry. This is currently being obtained by the *Kepler* satellite, and a stunning light curve of TrES-2 can already be inspected in Gilliland et al. (2010).

4.8   TrES-3

TrES-3 is one of the more massive TEPs ($M_{\rm b} = 1.91\,{\rm M}_{\rm Jup}$) and orbits a rather cool star ($T_{\rm eff} = 5650$ K) with an orbital period of only 1.3 d. It was identified as a TEP by O'Donovan et al. (2007) and a discovery-quality light curve has also been obtained by the SuperWASP survey (Collier Cameron et al. 2007). Follow-up transit photometry has been presented by Sozzetti et al. (2009) and Gibson et al. (2009), and occultation (secondary eclipse) observations have been secured by Winn et al. (2008a). A space-based light curve was obtained by the EPOXI mission (Ballard et al. 2009) but has not yet been published.

The O'Donovan et al. (2007) B- and z-band photometry of TrES-3 is of good quality, and the transit observations of the follow-up papers (Sozzetti et al. 2009; Gibson et al. 2009) are excellent. This, plus the fact that TrES-3 has a relatively low orbital inclination (82°), means that the light curve parameters can be obtained to an unusually high precision. In this work I analyse the B- and z-band data from O'Donovan et al. (2007), the $Vgri$-band observations from Sozzetti et al. (2009), and the Liverpool Telescope (LT) RISE measurements from Gibson et al. (2009). The last of the datasets, which has a passband of approximately $V+R$, was sorted in phase and then binned down by a factor of 20 (from 11 350 to 568 datapoints) to ease the computational burden.

For the solutions of the seven light curves I adopt those with both LD coefficients fixed for V, r and i, and the LD fit/fix solutions for the remainder (Fig. 12). Correlated noise is important for the V, g and LT datasets. For most of the datasets I find that the residual-permutation algorithm returns errorbars which are significantly asymmetric, with larger upper errorbars than lower errorbars for both $r_{\rm A}$ and $r_{\rm b}$, but that the Monte Carlo errorbars are close to symmetric. This implies that the red noise in the light curves is
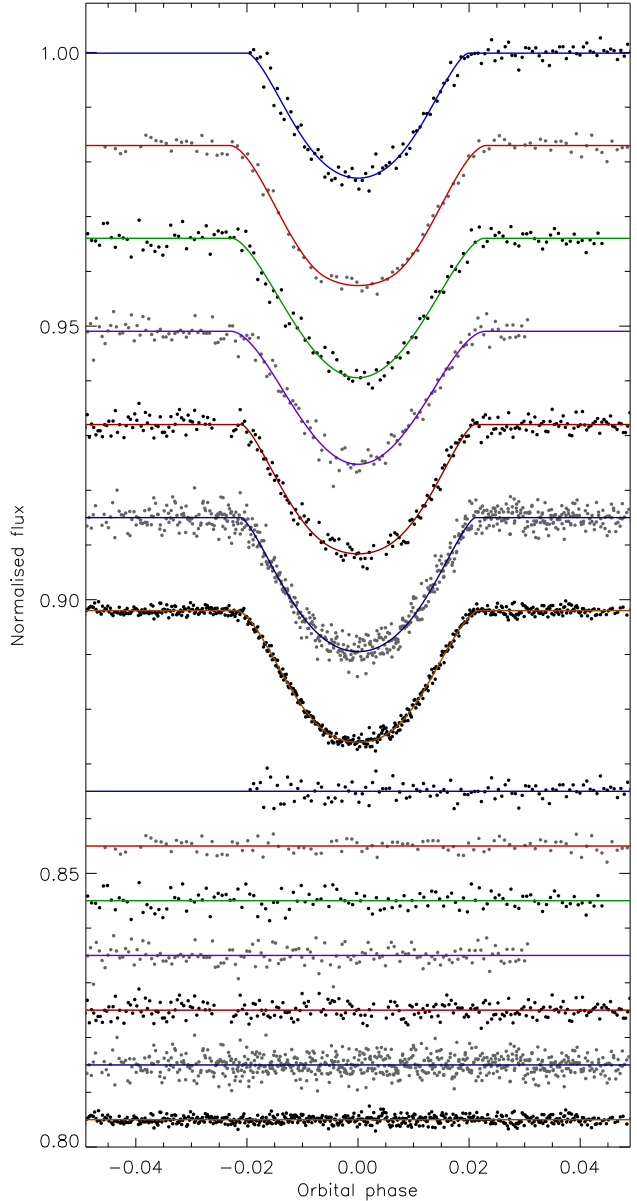

Figure 12. Phased light curves of the transits of TrES-3 compared to the best fits found using JKTEBOP and the quadratic LD law. Successive datasets and residuals are offset in flux for display purposes. From top to bottom are the B and z data (O'Donovan et al. 2007), $Vgri$ observations (Sozzetti et al. 2009) and LT $V+R$ measurements (Gibson et al. 2009).

biasing the results towards larger component radii, and would not have come to light if correlated noise was accounted for simply by rescaling the observational errors.

I accordingly end up with asymmetric errorbars for each light curve solution. The V and g solutions are quite uncertain and discrepant with the other results, so were rejected. To calculate the final photometric result I combined the solutions of the remaining five light curves by multiplying their probability density functions. The result is given in Table A36 and is found to be in good agreement with literature results.

The physical properties of the TrES-3 system are summarised in Table A37, and agree well with published values. For all five stellar model grids the best solution was found for zero age, and there is a possibility that edge effects will cause the uncertainties
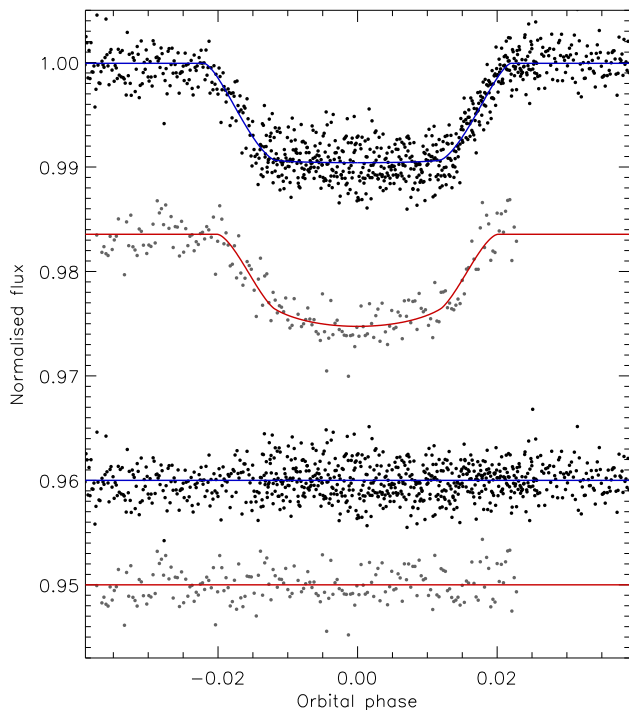
Figure 13. Phased light curves of the transits of TrES-4 compared to the best fits found using JKTEBOP and the quadratic LD law. The upper data are in the z band and the lower data are in the B band. The fits and residuals are offset in flux for display purposes.

Figure 14. Phased light curves of WASP-3 compared to the best fits found using JKTEBOP and the quadratic LD law. From top to bottom the light curves are LT $V+R$ (Gibson et al. 2008), which have been binned by a factor of ten for analysis, Keele R and IAC I (Pollacco et al. 2008). The residuals are offset from zero to the base of the figure.

to be slightly underestimated for this object (for an example of this phenomenon see HD 189733 in Paper I).

4.9   TrES-4

The planetary system TrES-4 was discovered by Mandushev et al. (2007), and is noteworthy for having a very hot ($T'_{\rm eq} = 1861$ K) and low-density ($0.15\,\rho_{\rm Jup}$) planet. Revised physical properties of the system have been presented by TWH08 and Sozzetti et al. (2009), and near-IR observations of the secondary eclipse show no evidence for orbital eccentricity (Knutson et al. 2009).

Like TrES-2 and WASP-2, high-resolution imaging observations by Daemgen et al. (2009) have detected a faint companion to TrES-4. It resides at an angular separation of 1.555 ± 0.005 arcsec and is fainter by $\Delta i = 4.560 \pm 0.017$ and $\Delta z = 4.232 \pm 0.025$ than TrES-4 A. These result in third light contributions of $L_3(i) = 0.0150 \pm 0.0002$ and $L3(z) = 0.0199 \pm 0.0005$, which are taken into account in the light curve analysis as described in Sect. 2.4.

In this work I study the high-precision B and z light curves presented in the discovery paper (Mandushev et al. 2007), and provide the first results to fully account for the third light contribution. Using ATLAS9 model spectra I have propagated the third light to the B-band, finding $L_3(B) = 0.0040 \pm 0.0003$ and a $T_{\rm eff} = 4206 \pm 78$ K for the companion star. The fainter star is more than twice as distant as TrES-4, so is not bound to the planetary system.

The B data are rather sparse and do not allow LD coefficients to be fitted for (Fig. 13). The z observations cover two transits so were studied with $P_{\rm orb}$ left as a fitted parameter; the LD fit/fix solutions were adopted. Correlated errors are important for both datasets. The two light curve solutions agree reasonably well (1.5σ)
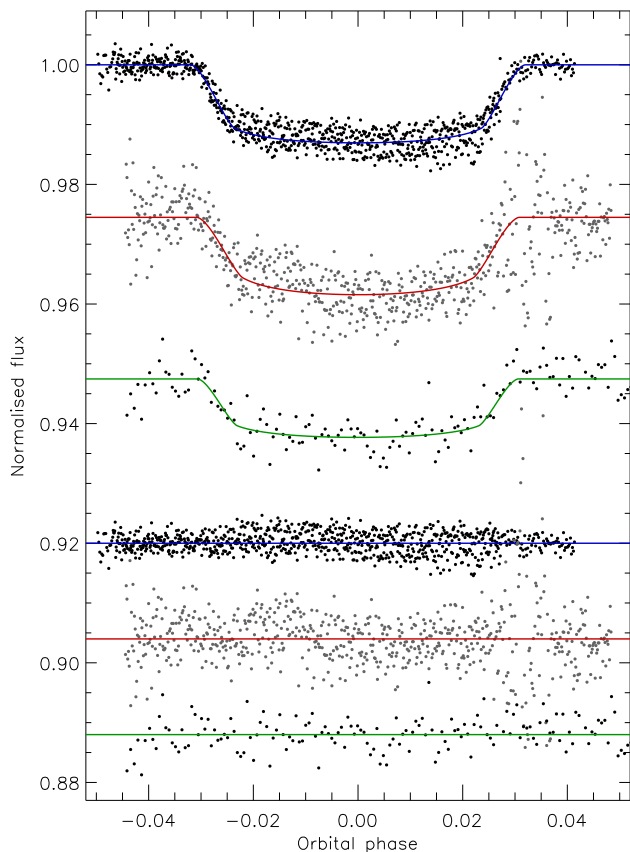
within the rather large errorbars, and were combined by weighted mean to find the final parameter values. This solution corresponds to a smaller i, and larger star and planet than found previously (Table A40). From Fig. 1 we would expect that accounting for third light would lead to a smaller $r_{\rm A}$ and larger $r_{\rm b}$ and i, which is only partially concordant with the current situation. The variation in parameter values must therefore be due to the different analysis methods used.

The physical properties of TrES-4 are given in Table A41 and conform to a more evolved star than found by previous studies, as expected for the larger $r_{\rm A}$ found above. The properties of the planet agree well with literature values, but are quite uncertain. The AB-SDIM error budget shows that an improved light curve and additional RV measurements would benefit this system. All four TEPs discovered by TrES have now been analysed in the current series of papers.

4.10   WASP-3

WASP-3 was identified as a possible TEP by Street et al. (2007) based on SuperWASP data (Pollacco et al. 2006). Confirmation of its planetary nature was provided by Pollacco et al. (2008), who presented four transit light curves obtained from various sources and found WASP-3 b to be one of the most strongly irradiated TEPs ($T'_{\rm eq} = 2028$ K). High-precision light curves from the LT have since been presented and analysed by Gibson et al. (2008). Here I

study these data, plus the Keele R-band and IAU 80 cm I-band observations from Pollacco et al. (2008). The other two light curves (IAC 80 cm V and SuperWASP) have either large systematics or a large scatter. I have binned consecutive sets of 10 datapoints of the LT light curve in order to limit CPU time; the sampling rate of the binned data is 30 s.

For the LT data I adopt the LD fit/fix results and find significantly larger errorbars from the residual-permutation analysis; correlated noise is clearly visible in these data in Fig. 14. The other two datasets also contain significant red noise, and the LD fixed solutions were adopted. The agreement between the three light curve solutions is excellent so they have been combined into a weighted mean (Table A45). Apart from a 2σ larger $r_{\rm b}$, the final values agree well with the studies of Pollacco et al. (2008) and Gibson et al. (2008) but not with the preliminary results given by Damasso et al. (2009).

The physical properties of the WASP-3 system were originally calculated using $K_{\rm A} = 251.2 \pm 9.3\,{\rm km\,s^{-1}}$ (Pollacco et al. 2008). After this work was completed a revised $K_{\rm A}$ of 276.0 ± 11.0 was presented by Simpson et al. (2009), who also found that the angle between the planetary orbit and the stellar spin was $\lambda = 15^{+10}_{-9}\,^{\circ}$. Shortly before the current work was submitted a further study of WASP-3 was produced (Tripathi et al. 2010), containing new results including $K_{\rm A} = 290.5^{+9.8}_{-9.2}\,{\rm km\,s^{-1}}$ and $\lambda = 3.3^{+2.5}_{-4.4}\,^{\circ}$.

The third and most recent $K_{\rm A}$ has been used to obtain the physical properties of the WASP-3 system (Table A46). I find that WASP-3 b has a rather larger mass and radius than most literature studies, except for that of Tripathi et al. (2010). More precise measurements of $T_{\rm eff}$ and $\left[\frac{\rm Fe}{\rm H}\right]$ for WASP-3 would be useful to improve our understanding of its physical properties. More extensive spectroscopy would also be useful to pin down $K_{\rm A}$, for which a variety of measurements are currently available.

4.11 WASP-10

WASP-10 was found to be a TEP system by Christian et al. (2009), and is notable for containing a fairly massive ($3.2\,{\rm M_{Jup}}$) planet transiting a small ($0.70\,{\rm R_\odot}$) and low-mass ($0.75\,{\rm M_\odot}$) star. The transit events are a generous 3.0% deep, so photometric follow-up of this system is comparatively easy. Christian et al. (2009) obtained data from the 0.8 m Tenagra and 1.2 m Mercator telescopes, but unfortunately none of the datasets cover a full transit event. High-precision follow-up photometry of one complete transit of WASP-10 was obtained by Johnson et al. (2009b), using a novel orthogonal frame transfer CCD (OPTIC) to shape the point spread function and thus obtain a scatter of only 0.5 mmag per datapoint at a reasonable sampling rate. I analyse the OPTIC observations to obtain the photometric parameters, and the Mercator data to provide a consistency check.

One complication for WASP-10 is its eccentric orbit. This is handled in the way described in Sect. 2.3, using the constraints $e\cos\omega = -0.045 \pm 0.02$ and $e\sin\omega = 0.023 \pm 0.04$ (Johnson et al. 2009b). For both light curves I find that correlated noise is unimportant and that the LD fit/fix solutions are best (Fig. 15). The two sets of results agree well (Table A49) and I adopt the OPTIC ones as final. The values agree well with those of Johnson et al. (2009b) but my errorbars are rather larger, due in part to the inclusion of several different LD laws rather than the reliance on only one. The agreement with Christian et al. (2009) is less good but still acceptable.

The ABSDIM analysis returns results (Table A50) which are again in good agreement with those of Johnson et al. (2009b) but
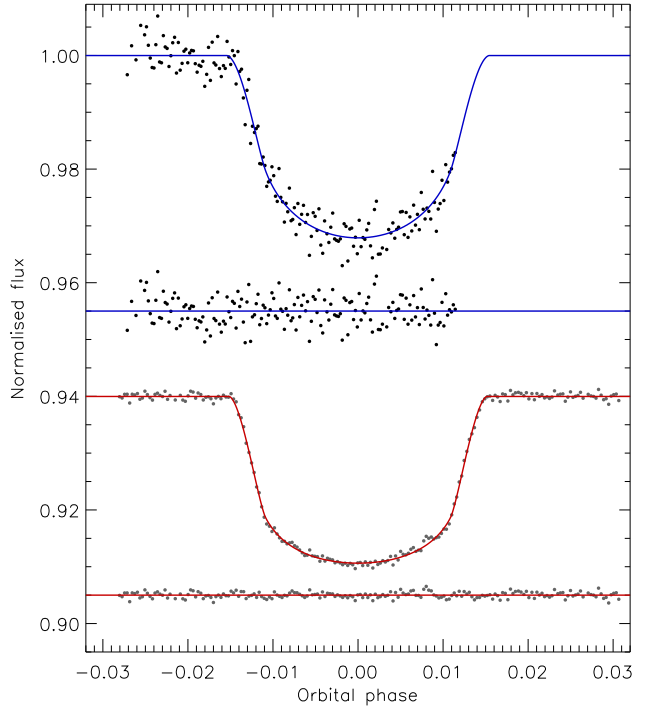

Figure 15. Phased light curves of WASP-10 compared to the best fit found using JKTEBOP and the quadratic LD law. The upper curve and residuals represent the Mercator data (Christian et al. 2009) and the lower curve and residuals are the OPTIC data (Johnson et al. 2009b). All offsets are additive in flux.

with larger errorbars. The agreement between different model sets is unusually poor for WASP-10, resulting in systematic errorbars which are a significant fraction of the random errorbars and as large as the total errorbars given by Johnson et al. Table A50 provides the first measurement of Θ for WASP-10 and also corrects a calculation error in the $T'_{\rm eq}$ listed in one of the published studies of this system. An improved photometric study of WASP-10 would settle the existing disagreement on its k value, and the system would also be favoured by more precise $T_{\rm eff}$ and $\left[\frac{\rm Fe}{\rm H}\right]$ measurements.

After the above study of WASP-10 was completed, new datasets on this star were presented by Dittmann et al. (2010) and Krejcova et al. (2010) and a disagreement over the system properties became manifest. The two new studies both prefer system properties similar to those of Christian et al. (2009) but discrepant with the results – based on a much better light curve – of Johnson et al. (2009b). This will be revisited in the future, once the newer data and perhaps further observations become available.

4.12 XO-2

The second planet discovered by the XO project (McCullough et al. 2006) is noteworthy for having a parent star which is very metal-rich ($\left[\frac{\rm Fe}{\rm H}\right] = 0.45$) and a member of a common proper motion binary system (Burke et al. 2007). Good transit light curves from the Perkins telescope were published in the discovery paper (McCullough et al. 2006), and from the FLWO 1.2 m by the Transit Light Curve Project (Fernandez et al. 2009). The system has also been observed as part of the NASA EPOXI mission (Ballard et al. 2009).

In this work I analyse the Perkins and FLWO observations (Fig. 16). In the former case correlated noise is important and in
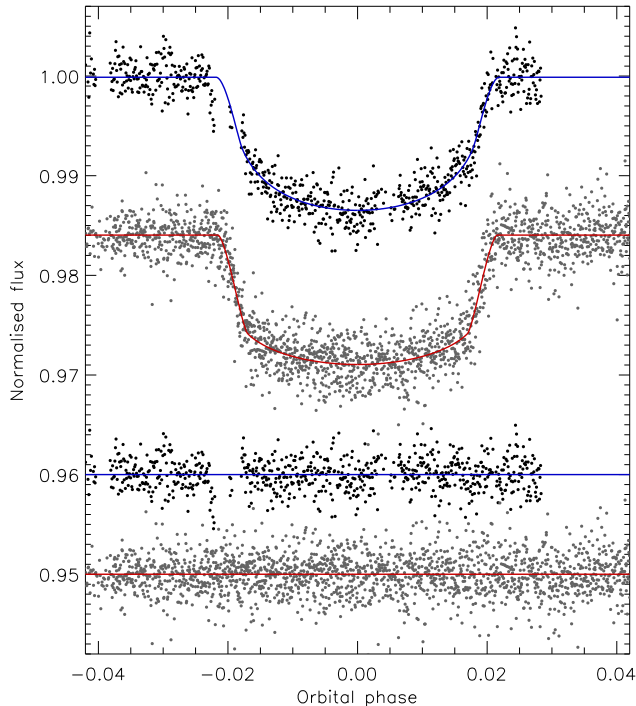
Figure 16. Phased light curves of XO-2 compared to the best fits found using JKTEBOP and the quadratic LD law. The upper light curve is R-band from the Perkins telescope (Burke et al. 2007) and the lower one is z-band from the FLWO 1.2 m telescope (Fernandez et al. 2009). The residuals are offset from zero to the base of the figure.

the latter it is not. I adopt the LD fit/fix results for both datasets and combine their probability density functions to find the final results. The solutions have $i \sim 90°$ and thus asymmetric errorbars. The agreement between the two light curves and versus published values is good (Table A53).

The ABSDIM analysis is complicated by the high $\left[\frac{Fe}{H}\right]$ (Table A54). The results using the five different theoretical models are scattered, giving systematic errors which are larger than the statistical ones for the two most-affected quantities, M_A and a. However, the agreement with other studies is good. A more precise K_A value would be profitable.

4.13 XO-3

XO-3 was discovered by Johns-Krull et al. (2008) to be a TEP which is so massive it is near the $13\,M_{Jup}$ value which represents the minimum mass of a brown dwarf. Johns-Krull et al. (2008) presented two alternative sets of physical properties for the system, the first of which put XO-3 b at $13.25 \pm 0.64\,M_{Jup}$ but yielded a relatively poor fit to the observed transit light curve. The second set ignored the spectroscopic measurement of $\log g_A$, yielding $M_2 = 12.03 \pm 0.46\,M_{Jup}$ and a much better fit to the light curve. The latter solution is preferable because light curve shapes are more reliable than spectroscopically-derived surface gravities for late-type dwarf stars.

A follow-up study of XO-3 was presented by Winn et al. (2008b), based on high-quality new light curves and also ignoring the spectroscopic $\log g_A$. Additional observations have been presented by Winn et al. (2009). In this work I analyse the z-band photometry obtained by Winn et al. (2008b) using the FLWO 1.2 m,
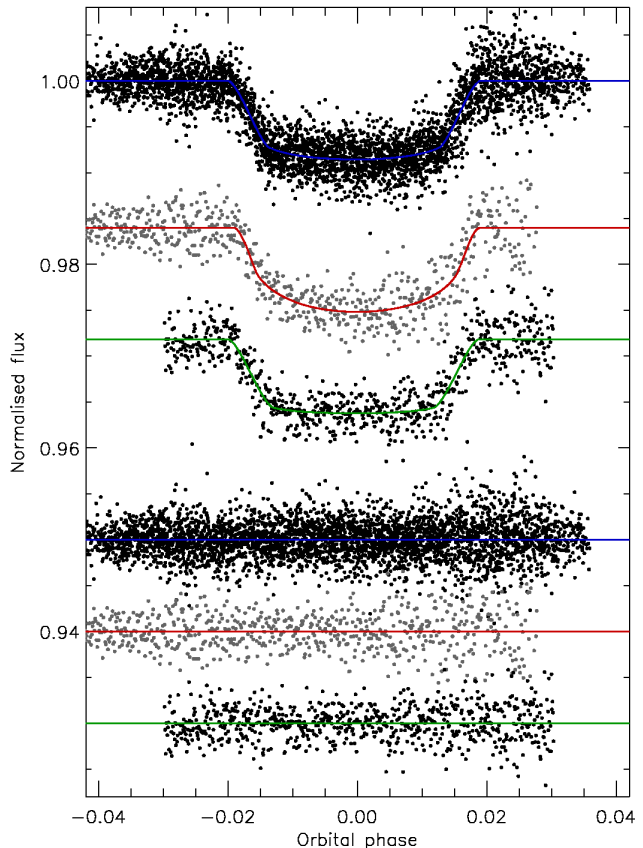

Figure 17. Phased light curves of XO-3 compared to the best fits found using JKTEBOP and the quadratic LD law. From top to bottom the light curves are KeplerCam z-band (Winn et al. 2008b), and KeplerCam r-band and FLWO I-band (Winn et al. 2009). The residuals are offset from zero.

and the r-band FLWO 1.2 m and I-band Nickel datasets presented by Winn et al. (2009). The photometric observations presented by Johns-Krull et al. (2008) are not included because they comprise many datasets of only moderate quality.

An important property of XO-3 is its substantial orbital eccentricity ($e = 0.28$), which is a common feature of the more massive planets (Southworth et al. 2009c) and might indicate that they are a different population of objects to their less massive cousins. XO-3 is also known to exhibit a large spin-orbit misalignment (Hébrard et al. 2008; Winn et al. 2009) suggestive of dynamical evolution through gravitational interactions (e.g. Fabrycky & Winn 2009). In the following analysis I adopt the constraints $e = 0.2884 \pm 0.0035$ and $\omega = 346.3 \pm 1.3$, taken from Winn et al. (2009). Compared to a solution assuming a circular orbit, r_A and r_b decrease by 0.0033 and 0.00029 respectively, which is less than 1σ in both cases.

Correlated errors are unimportant for all three light curves, and in each case the best solutions are LD fit/fix. The z and I data agree well but the r results have a higher i and a 2.5σ lower r_A (Table A58). The most extensive dataset is z, so I have combined the results from this and I and rejected the r results as discrepant. The best fits are plotted in Fig 17. My results agree well with those of Winn et al. (2009) and with the second of the two alternative solutions given by Johns-Krull et al. (2008).

When determining the physical properties of the XO-3 system I adopted increased uncertainties of 75 K in T_{eff} and 0.05 dex in $\left[\frac{Fe}{H}\right]$, to allow for the possibility of systematic errors in these
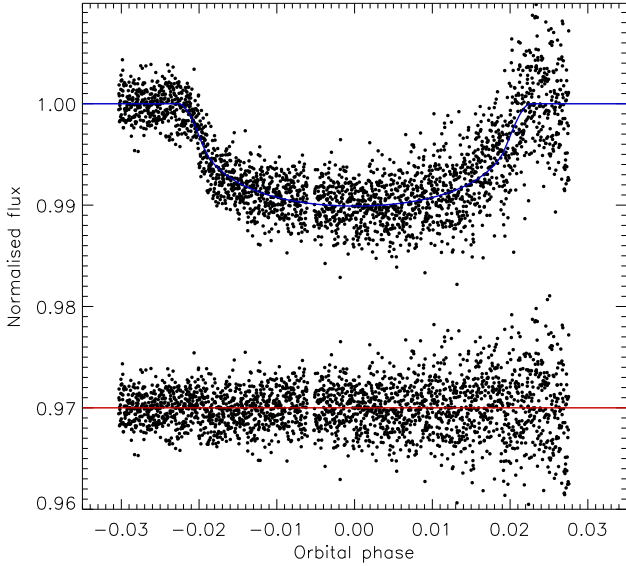
Figure 18. Phased light curve of XO-4 from the Perkins telescope (McCullough et al. 2008). The blue line shows the best fit from JKTEBOP using the quadratic LD law. The residuals are offset from zero.

values for low-mass stars such as XO-3 A, and to account for the low spectroscopic gravity value (3.95 ± 0.06 versus 4.23 ± 0.04) in the discovery paper (Johns-Krull et al. 2008). Like the JKTE-BOP outcome, the results of the ABSDIM analysis agree well with those of Winn et al. (2009) but not with the preferred solution of Johns-Krull et al. (2008). The mass of the planet is $M_{\rm b} = 11.8 \pm 0.5\,M_{\rm Jup}$, which is close to but below the $13\,M_{\rm Jup}$ dividing line between planets and brown dwarfs. The *VRSS* model results disagree strongly with those of the other models, so were not included in the final analysis. The $T'_{\rm eq}$ of XO-3 b is high at 1729 ± 34 K, making it an interesting object for the study of planetary atmospheres. Aside from the *VRSS* models, XO-3 is one of the best-measured TEPs. An improved spectroscopic study, incorporating the best $\log g_{\rm A}$ value given in Table A59, would be the best way of improving this understanding even further.

4.14 XO-4

XO-4 was discovered to be a TEP by McCullough et al. (2008); the parent star is one of the hottest of the known planetary hosts. Here I analyse the R-band Perkins telescope light curve obtained by McCullough et al. (2008). Correlated errors are unimportant and the best solutions are LD fit/fix. The inclination is near $90°$, resulting in asymmetric errorbars. My photometric solution (Fig. 18) is in excellent agreement with that of McCullough et al. (Table A61).

The results of the ABSDIM analysis are given in Table A62, and include the first reported measurements of the $T'_{\rm eq}$, Safronov number, $g_{\rm b}$, $\rho_{\rm A}$ and $\rho_{\rm b}$ of the XO-4 system. The other output parameters agree well with those of McCullough et al. (2008); $M_{\rm b}$ is $0.2\,M_{\rm Jup}$ smaller in my solution but this is within the errorbars. Improved photometric and RV observations of XO-4 would be beneficial.

4.15 XO-5

The discovery that XO-5 is a TEP system was presented by Burke et al. (2008) and extensive follow-up observations in the
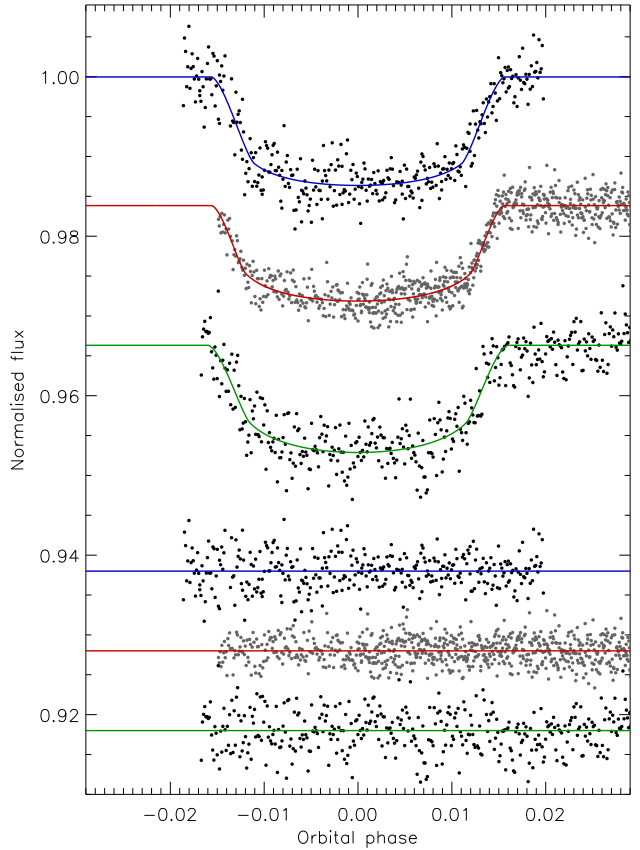

Figure 19. Phased light curves of XO-5 compared to the best fits found using JKTEBOP and the quadratic LD law. From top to bottom the light curves are Perkins R-band (Burke et al. 2008), and KeplerCam i-band and z-band (Pál et al. 2009). The residuals are offset from zero.

context of the HAT consortium were presented by Pál et al. (2009). I adopt the $K_{\rm A}$ value from Pál et al. (2009), which agrees with but is much more precise than that given by Burke et al. (2008). A comparison of the $T_{\rm eff}$ and $\left[\frac{\rm Fe}{\rm H}\right]$ given by the two studies shows a concerning disagreement, which may be due to the treatment of $\log g_{\rm A}$. Pál et al. (2009) fix $\log g_{\rm A}$ at the transit-derived value during their spectral synthesis analysis, and also have spectra with a higher signal to noise ratio, so I have preferred their spectroscopic results.

Three high-quality light curves of XO-5 are available: R-band coverage of one full transit using the Perkins telescope (Burke et al. 2008), and i- and z-band observations (both covering one full and one partial transit) obtained with the FLWO 1.2 m telescope (Pál et al. 2009). I have analysed all three datasets, and the best fits are shown in Fig. 19. In the case of the R and z data correlated noise is important, and in all cases the best solutions are LD fit/fix. The resulting photometric parameters are in good agreement except for k, for which there is a large scatter of 5σ (Table A66). The three parameter sets have therefore been combined and the errorbar in k increased to account for this discrepancy.

The physical properties of XO-5 are given in Table A67, and are in good agreement with established values. This system is a good candidate for improved photometric observations, which would allow to sort out the discrepancy in k and improve the precision of the system properties.

4.16 TEPs studied in previous papers

The preceding subsections have presented full studies of fifteen TEPs. In this subsection I apply my improved ABSDIM analysis to the other fifteen systems for which photometric results have already been calculated (Paper I; Southworth et al. 2009a,b,c, 2010). Their physical properties are collected and compared to literature results in Tables A68 to A81, and relevant points are discussed below.

GJ 436. Attempts to obtain solutions for $T_{\mathrm{eff}} = 3350\,\mathrm{K}$ failed. Inspection of Fig. 4 explains this: for a $0.5\,\mathrm{M_\odot}$ star we expect T_{eff} values in the range 3500–4000 K (except for the *Claret* models which prefer 3100 K). I have therefore adopted the higher T_{eff} of 3500 K from Bean et al. (2006), with an errorbar doubled to 100 K. The results with the *Claret* models are discrepant so were not incorporated into the final solution. This does not mean that the *Claret* models are wrong – they are in fact closer to the measured properties of eclipsing binaries (primarily CM Dra) in this mass regime – but that they depart from the consensus established by the other model sets. The lesson here is that we require an improved understanding of low-mass stars to better measure the physical properties of the important GJ 436 system. The revised results for GJ 436 (Table A68) are slightly smaller than those found in Paper II, and are in good agreement with literature studies.

HAT-P-1. I used a new K_{A} value from Johnson et al. (2008). My ABSDIM solutions prefer the T_{eff} value used in Paper II (Bakos et al. 2007a) to the higher one found by Ammler-von Eiff et al. (2009).

HD 189733. A new K_{A} value is available from Boisse et al. (2009), supported by the value given by Triaud et al. (2009). The ABSDIM solutions with different models converged on either a very young ($\sim$1 Gyr) or old (9–13 Gyr) age, resulting in large systematic errorbars for most output parameters. HD 189733 is an active star (Bouchy et al. 2005b) with starspots (Pont et al. 2007), a short rotation period of 12 d (Winn et al. 2007b), RV jitter (Boisse et al. 2009), and Ca H & K emission modulated on its rotation period (Moutou et al. 2007). These facts imply a young age (Skumanich 1972; Mamajek & Hillenbrand 2008) so the search for the best solution was restricted to ages below 5 Gyr. This resulted in much more consistent solutions, with ages of 0.1–2.9 Gyr, which were accepted as the final results (Table A70).

HD 209458. I used the revised value of $K_{\mathrm{A}} = 84.67 \pm 0.70$ given by TWH08. The revised results are in good agreement with those from Paper II. R_{A} has been measured directly by interferometric means (van Belle & von Braun 2009) to be 2σ larger than found here and in all other studies of this object given in Table A71.

OGLE-TR-10. The light curve solution used in Paper II was unintentionally a preliminary rather than the final one from Paper I. This has been corrected here, resulting in a less dense planet. The properties of OGLE-TR-10 are rather uncertain and the system is badly in need of improved spectroscopy and photometry.

OGLE-TR-132. I use the more precise K_{A} value of $167 \pm 18\,\mathrm{km\,s^{-1}}$ given by Moutou et al. (2004) which was overlooked in Papers I and II. OGLE-TR-132 b has a high T'_{eq} of 2017 ± 97 K (Table 75).

WASP-2. The results for this system are reproduced from the dedicated study of Southworth et al. (2010).

WASP-4, WASP-5, WASP-18. I use the new and improved K_{A} values for these three TEPs from Triaud et al. (2010).

5 TRACKING THE SYSTEMATIC ERRORS IN THE PROPERTIES OF TRANSITING SYSTEMS

A major result of the current work is a detailed understanding of where model-dependent systematic errors surface in the analysis of TEPs, and the importance of these systematics for the various physical properties which can be calculated. The approach used in this work means that all of the model dependence is combined into K_{b} (the velocity amplitude of the planet), making it an excellent tracer of systematic errors. For each TEP a separate value of K_{b} is found using each of the five sets of stellar models, as well as for the empirical mass–radius relation (Paper II). I have converted these into 'consensus values', $\langle K_{\mathrm{b}} \rangle$, using the same algorithm as for the other measured physical properties: the unweighted mean of the values from the five different stellar model sets. Remember that $\langle K_{\mathrm{b}} \rangle$ should not be taken as an indicator of *correctness*, only of concordance.

From Eqs. 4 to 12 in Paper II it can be seen that the component masses are most sensitive to systematic errors ($M_{\mathrm{A}} \propto K_{\mathrm{b}}^3$ and $M_{\mathrm{b}} \propto K_{\mathrm{b}}^2$) and that their radii, gravities and densities are less so (all directly proportional to K_{b}). The semimajor axis is also rather model-dependent as the other quantities required to calculate it all have much smaller uncertainties than K_{b} does.

A detailed exploration of model-dependence is presented in Fig. 20 as a function of T_{eff}, $\left[\frac{\mathrm{Fe}}{\mathrm{H}}\right]$ and M_{A}. The top panels in this Figure highlight the generally good agreement between different model sets. The mass–radius relation is in much poorer agreement and is biased to high values as it does not account for the effects of evolution through the main-sequence phase (particularly apparent for HAT-P-2, TrES-4 and XO-3). This bias to large K_{b} comes from trying to reproduce the low density of an evolved star, and pushes the mass and radius of the planet and star to high and incorrect values.

Turning to the stellar model sets in Fig. 20, clear trends with respect to T_{eff}, $\left[\frac{\mathrm{Fe}}{\mathrm{H}}\right]$ and M_{A} can be seen in many cases. The *Claret* models yielded larger K_{b} values on average, particularly for low values of T_{eff} and $\left[\frac{\mathrm{Fe}}{\mathrm{H}}\right]$. This predilection for high values is balanced by other model sets: the *Teramo* and *VRSS* models both tend to produce lower K_{b} values and the *DSEP* models trend to low K_{b} for cooler and more metal-poor stars. Within this mélange, the Y^2 models are the closest to the consensus value and do not exhibit significant trends with the stellar properties. The Y^2 models are thus the best choice to obtain quick results, although of course other model sets are required for the assessment of systematic errors.

Figs. 21 and 22 compare the sizes of the random and systematic errors in stellar mass, as a function of M_{A} and of $\left[\frac{\mathrm{Fe}}{\mathrm{H}}\right]$, respectively. M_{A} was chosen for this comparison because it is one of the parameters more affected by systematics; it was also expected that these systematic effects would be minimised in the region of $1\,\mathrm{M_\odot}$ and $\left[\frac{\mathrm{Fe}}{\mathrm{H}}\right] = 0$ as all of the stellar model sets are calibrated on the Sun. Surprisingly, this does not turn out to be the case. There is a hard lower limit of 1% on the errors in M_{A} arising from model-dependent systematics, but this lower limit is reached at a wide range of masses and $\left[\frac{\mathrm{Fe}}{\mathrm{H}}\right]$ values. The systematic errors are clearly larger for lower-mass stars ($<0.9\,\mathrm{M_\odot}$) and for a high metal abundance ($\left[\frac{\mathrm{Fe}}{\mathrm{H}}\right] > 0.4$). The hard lower limit is unavoidable until stellar model sets are in much better agreement, and the mass–radius relation results hint that the real systematic errors are probably somewhat higher than this. The random errors in M_{A} tend to decrease towards higher masses (temporarily ignoring the much fainter OGLE systems), as expected because more massive stars are intrinsically brighter and therefore easier to obtain good data for.
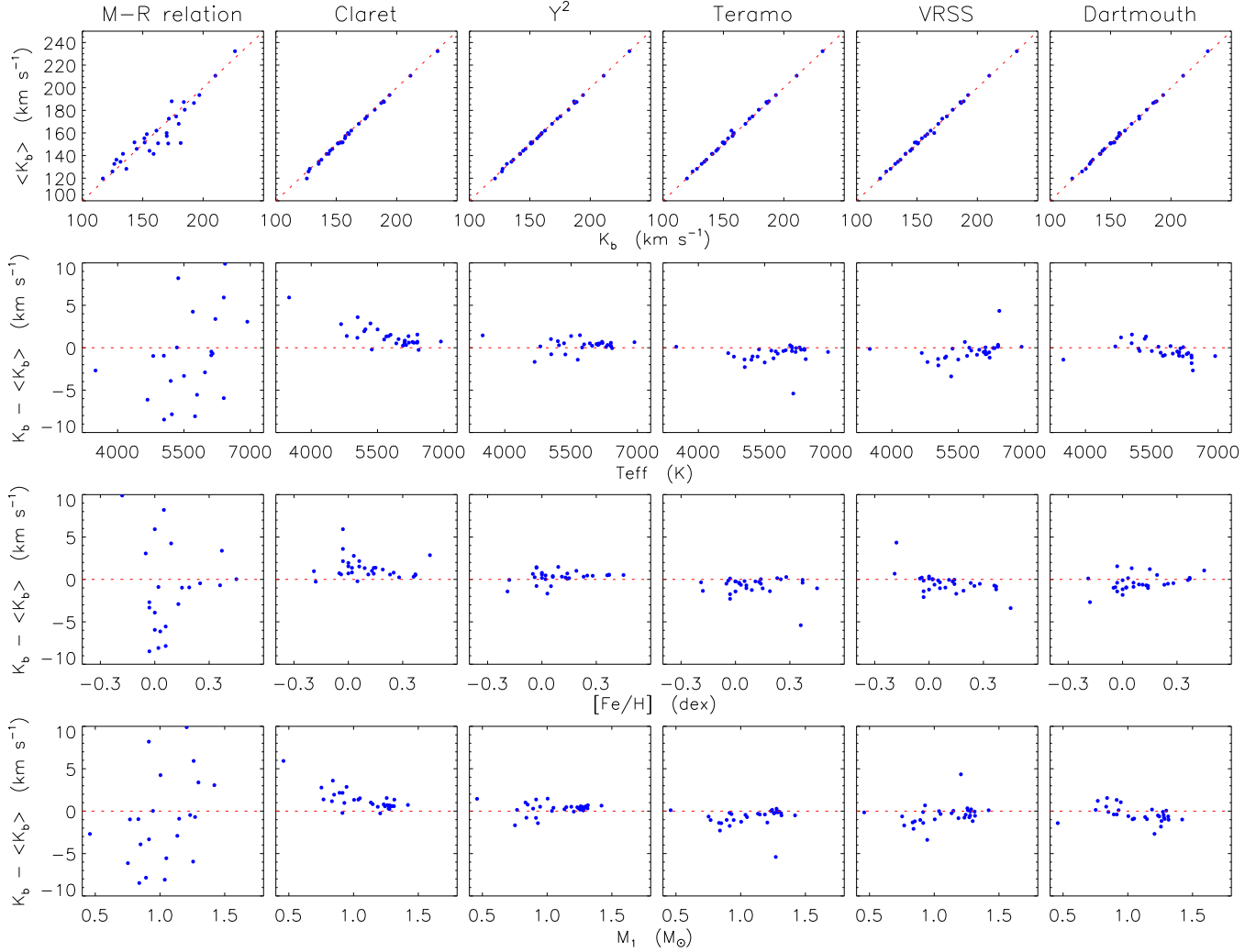
Figure 20. Comparisons between the $K_{\rm b}$ values obtained using specific sets of stellar evolutionary models and the unweighted mean value, $\langle K_{\rm b} \rangle$, for each TEP. From left to right the panels show results for the mass–radius relation and then the five stellar model sets. The top panels compare $K_{\rm b}$ to $\langle K_{\rm b} \rangle$ for each model set, with parity indicated by a dotted line. Lower panels show the difference ($K_{\rm b} - \langle K_{\rm b} \rangle$) as functions of effective temperature, metal abundance and stellar mass. Errorbars have been ignored for clarity; their median values are $\pm 3\,{\rm km\,s^{-1}}$ (statistical) and $\pm 1.4\,{\rm km\,s^{-1}}$ (systematic).

5.1 An external test: WASP-11 versus HAT-P-10

One of the best ways to investigate the presence of systematic errors is to compare two independent studies of the same object. Whilst multiple discovery and characterisation publications have been presented for several TEPs (e.g. XO-1 and XO-5), successive papers on these objects have in each case been informed by the initial discovery papers. There are two exceptions: HD 80606 and WASP-11 / HAT-P-10. In the case of HD 80606 three groups discovered its transiting nature essentially simultaneously, but their analyses were heavily dependent on the same published spectroscopic observations. WASP-11 / HAT-P-10 is therefore the only TEP which was discovered and fully characterised by two groups working without knowledge of each others' analyses. The discovery papers were submitted within a week of each other, but the agreed name of the system is WASP-11 / HAT-P-10 because the WASP group submitted their paper first.

In Table 4 I collect the properties of WASP-11 determined in the two discovery papers (West et al. 2009; Bakos et al. 2009). The values in general show a gratifying agreement, but two quantities
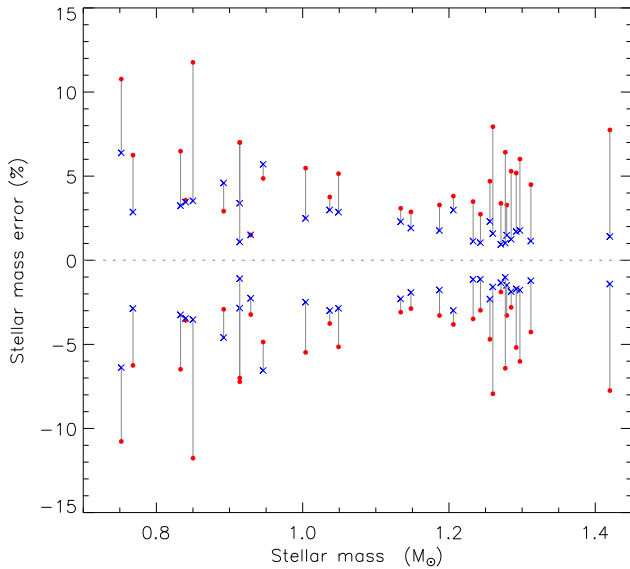
stand out as being discrepant to some extent. The $T_{\rm eff}$ values disagree by 1.6σ and the k values by 2.7σ. The divergent k values have a large knock-on effect on the planetary properties ($R_{\rm b}$, $g_{\rm b}$ and $\rho_{\rm b}$).

The possibility of systematic errors in $T_{\rm eff}$ is a well-known phenomenon (see Sect. 3), so the 1.6σ disagreement is unsurprising. Similarly, k measurements primarily depend on the observed transit depth (see Sect. 2) and can be affected by imperfect normalisation as well as by astrophysical effects such as starspots. Discrepancies in k have previously been found in the well-studied systems HD 189733 and HD 209458 (Paper I), WASP-4 (Southworth et al. 2009b), HAT-P-1 and WASP-10 (Sections 4.1 and 4.11).

This implies that a high-quality study of a TEP cannot rely on photometric coverage of only one transit, irrespective of its quality, but must include observations of two or preferably more in order to pick up on well-camouflaged systematic errors affecting light curves. It is important to realise that a systematic over- or underestimation of a transit depth has a big effect on measurements of the planet properties, but cannot be identified in any dataset covering only one transit.

Table 5. Physical properties of the stellar components of the TEPs studied in this work. For each quantity the first uncertainty is derived from a propagation of all observational errors and the second uncertainty is an estimate of the systematic errors arising from the dependence on stellar theory.

System	Semimajor axis (AU)	Mass ($M_\odot$)	Radius ($R_\odot$)	$\log g_A$ [cm/s]	Density ($\rho_\odot$)	Age (Gyr)
GJ 436	$0.02887 \pm 0.00089 \pm 0.00035$	$0.459 \pm 0.043 \pm 0.017$	$0.454 \pm 0.029 \pm 0.005$	$4.787 \pm 0.030 \pm 0.005$	4.92 ± 0.55	unconstrained
HAT-P-1	$0.05535 \pm 0.00057 \pm 0.00042$	$1.134 \pm 0.035 \pm 0.026$	$1.112 \pm 0.031 \pm 0.008$	$4.400 \pm 0.024 \pm 0.003$	0.824 ± 0.066	$2.1^{+1.4\ +0.5}_{-1.2\ -0.6}$
HAT-P-2	$0.06740 \pm 0.00074 \pm 0.00034$	$1.279 \pm 0.042 \pm 0.019$	$1.68\ \pm 0.15\ \pm 0.01$	$4.092 \pm 0.074 \pm 0.002$	0.268 ± 0.070	$2.6^{+0.4\ +0.5}_{-0.7\ -0.3}$
HD 149026	$0.04288^{+0.00048\ +0.00013}_{-0.00027\ -0.00019}$	$1.271^{+0.043\ +0.012}_{-0.024\ -0.017}$	$1.290^{+0.120\ +0.004}_{-0.058\ -0.006}$	$4.321^{+0.042\ +0.001}_{-0.070\ -0.002}$	$0.592^{+0.083}_{-0.129}$	$1.2^{+1.1\ +0.3}_{-1.5\ -0.1}$
HD 189733	$0.03142 \pm 0.00038 \pm 0.00036$	$0.840 \pm 0.030 \pm 0.029$	$0.752 \pm 0.023 \pm 0.009$	$4.610 \pm 0.026 \pm 0.005$	1.98 ± 0.17	$1.4^{+4.7\ +1.5}_{-1.4\ -1.3}$
HD 209458	$0.04747 \pm 0.00046 \pm 0.00031$	$1.148 \pm 0.033 \pm 0.022$	$1.162 \pm 0.012 \pm 0.008$	$4.368 \pm 0.005 \pm 0.003$	0.733 ± 0.008	$2.3^{+0.9\ +0.5}_{-0.7\ -0.4}$
OGLE-TR-10	$0.04516 \pm 0.00099 \pm 0.00015$	$1.277 \pm 0.082 \pm 0.013$	$1.52\ \pm 0.10\ \pm 0.00$	$4.178 \pm 0.053 \pm 0.001$	0.361 ± 0.063	$3.1^{+3.3\ +0.3}_{-0.7\ -0.2}$
OGLE-TR-56	$0.02386 \pm 0.00028 \pm 0.00009$	$1.233 \pm 0.043 \pm 0.014$	$1.26\ \pm 0.14\ \pm 0.00$	$4.331 \pm 0.094 \pm 0.002$	0.62 ± 0.21	$1.7^{+1.4\ +0.3}_{-2.0\ -0.2}$
OGLE-TR-111	$0.04651 \pm 0.00099 \pm 0.00051$	$0.833 \pm 0.054 \pm 0.027$	$0.842 \pm 0.042 \pm 0.009$	$4.508 \pm 0.044 \pm 0.005$	1.40 ± 0.19	unconstrained
OGLE-TR-113	$0.02278 \pm 0.00047 \pm 0.00022$	$0.768 \pm 0.048 \pm 0.022$	$0.780 \pm 0.029 \pm 0.008$	$4.539 \pm 0.028 \pm 0.004$	1.62 ± 0.13	unconstrained
OGLE-TR-132	$0.03029 \pm 0.00062 \pm 0.00018$	$1.297 \pm 0.078 \pm 0.023$	$1.37\ \pm 0.14\ \pm 0.01$	$4.275 \pm 0.083 \pm 0.003$	0.50 ± 0.15	$1.5^{+4.2\ +0.3}_{-1.5\ -0.4}$
OGLE-TR-182	$0.05205 \pm 0.00057 \pm 0.00031$	$1.187 \pm 0.039 \pm 0.021$	$1.53\ \pm 0.17\ \pm 0.01$	$4.142 \pm 0.089 \pm 0.003$	0.33 ± 0.10	$4.3^{+0.5\ +1.4}_{-1.9\ -1.3}$
OGLE-TR-211	$0.05105^{+0.00076\ +0.00020}_{-0.00073\ -0.00021}$	$1.312^{+0.058\ +0.015}_{-0.056\ -0.016}$	$1.56^{+0.18\ +0.01}_{-0.10\ -0.01}$	$4.170^{+0.052\ +0.002}_{-0.085\ -0.002}$	$0.345^{+0.068}_{-0.090}$	$2.6^{+0.6\ +0.4}_{-0.7\ -0.3}$
OGLE-TR-L9	$0.0404\ \pm 0.0011\ \pm 0.0002$	$1.42\ \pm 0.11\ \pm 0.02$	$1.503 \pm 0.083 \pm 0.008$	$4.236 \pm 0.043 \pm 0.002$	0.418 ± 0.061	$1.0^{+0.6\ +0.3}_{-0.7\ -0.2}$
TrES-1	$0.03946 \pm 0.00039 \pm 0.00060$	$0.892 \pm 0.026 \pm 0.041$	$0.818 \pm 0.017 \pm 0.013$	$4.563 \pm 0.019 \pm 0.007$	1.632 ± 0.092	$3.4^{+3.4\ +1.9}_{-3.0\ -2.9}$
TrES-2	$0.03635 \pm 0.00063 \pm 0.00035$	$1.049 \pm 0.054 \pm 0.030$	$1.002 \pm 0.029 \pm 0.010$	$4.457 \pm 0.027 \pm 0.004$	1.043 ± 0.088	$2.5^{+2.8\ +0.7}_{-2.5\ -0.8}$
TrES-3	$0.02283^{+0.00012\ +0.00012}_{-0.00025\ -0.00017}$	$0.929^{+0.014\ +0.014}_{-0.030\ -0.021}$	$0.818^{+0.004\ +0.004}_{-0.013\ -0.006}$	$4.581^{+0.007\ +0.002}_{-0.010\ -0.003}$	$1.700^{+0.047}_{-0.051}$	$0.1^{+0.7\ +0.0}_{-0.0\ -0.0}$
TrES-4	$0.04965 \pm 0.00087 \pm 0.00028$	$1.292 \pm 0.067 \pm 0.022$	$1.92\ \pm 0.11\ \pm 0.01$	$3.981 \pm 0.047 \pm 0.002$	0.182 ± 0.030	$3.7^{+1.6\ +0.2}_{-1.4\ -0.4}$
WASP-1	$0.03898^{+0.00036\ +0.00013}_{-0.00039\ -0.00014}$	$1.243^{+0.034\ +0.013}_{-0.037\ -0.014}$	$1.455^{+0.052\ +0.005}_{-0.079\ -0.005}$	$4.207^{+0.045\ +0.002}_{-0.028\ -0.002}$	$0.403^{+0.069}_{-0.037}$	$3.0^{+0.7\ +0.3}_{-0.6\ -0.3}$
WASP-2	$0.03033 \pm 0.00060 \pm 0.00043$	$0.803 \pm 0.049 \pm 0.034$	$0.807 \pm 0.019 \pm 0.011$	$4.529 \pm 0.017 \pm 0.006$	1.527 ± 0.067	$11.9^{+8.1\ +3.3}_{-4.3\ -2.5}$
WASP-3	$0.03187 \pm 0.00086 \pm 0.00020$	$1.26\ \pm 0.10\ \pm 0.02$	$1.377 \pm 0.085 \pm 0.009$	$4.262 \pm 0.044 \pm 0.003$	0.484 ± 0.073	$2.1^{+1.5\ +0.4}_{-1.2\ -0.3}$
WASP-4	$0.02307^{+0.00053\ +0.00026}_{-0.00055\ -0.00022}$	$0.914^{+0.064\ +0.031}_{-0.066\ -0.026}$	$0.905^{+0.021\ +0.010}_{-0.022\ -0.009}$	$4.485^{+0.011\ +0.005}_{-0.012\ -0.004}$	$1.233^{+0.020}_{-0.022}$	$7.0^{+5.2\ +2.1}_{-4.5\ -1.8}$
WASP-5	$0.02714 \pm 0.00049 \pm 0.00022$	$1.004 \pm 0.055 \pm 0.025$	$1.077 \pm 0.042 \pm 0.009$	$4.375 \pm 0.030 \pm 0.004$	0.803 ± 0.080	$7.0^{+3.2\ +1.5}_{-3.0\ -1.5}$
WASP-10	$0.0378\ \pm 0.0014\ \pm 0.0008$	$0.752 \pm 0.081 \pm 0.048$	$0.703 \pm 0.036 \pm 0.015$	$4.620 \pm 0.049 \pm 0.009$	2.16 ± 0.31	unconstrained
WASP-18	$0.02034 \pm 0.00032 \pm 0.00016$	$1.256 \pm 0.059 \pm 0.029$	$1.222 \pm 0.042 \pm 0.010$	$4.363 \pm 0.027 \pm 0.003$	0.689 ± 0.062	$0.5^{+1.2\ +0.6}_{-0.9\ -0.4}$
XO-1	$0.04944 \pm 0.00062 \pm 0.00050$	$1.037 \pm 0.039 \pm 0.031$	$0.942 \pm 0.022 \pm 0.009$	$4.506 \pm 0.021 \pm 0.004$	1.242 ± 0.080	$0.9^{+2.4\ +0.8}_{-0.9\ -0.8}$
XO-2	$0.03647^{+0.00059\ +0.00069}_{-0.00058\ -0.00081}$	$0.946^{+0.046\ +0.054}_{-0.046\ -0.062}$	$0.970^{+0.028\ +0.018}_{-0.035\ -0.022}$	$4.440^{+0.037\ +0.008}_{-0.021\ -0.010}$	$1.037^{+0.128}_{-0.058}$	$1.9^{+4.5\ +4.7}_{-1.9\ -1.9}$
XO-3	$0.04529 \pm 0.00057 \pm 0.00045$	$1.206 \pm 0.046 \pm 0.036$	$1.409 \pm 0.054 \pm 0.014$	$4.222 \pm 0.027 \pm 0.004$	0.431 ± 0.041	$3.0^{+0.9\ +0.5}_{-0.6\ -0.4}$
XO-4	$0.05475^{+0.00094\ +0.00022}_{-0.00051\ -0.00035}$	$1.285^{+0.068\ +0.016}_{-0.036\ -0.024}$	$1.530^{+0.362\ +0.006}_{-0.069\ -0.010}$	$4.178^{+0.034\ +0.002}_{-0.169\ -0.002}$	$0.359^{+0.046}_{-0.160}$	$2.7^{+0.6\ +0.2}_{-0.5\ -0.3}$
XO-5	$0.0494\ \pm 0.0011\ \pm 0.0002$	$0.914 \pm 0.064 \pm 0.010$	$1.065 \pm 0.064 \pm 0.004$	$4.344 \pm 0.043 \pm 0.002$	0.76 ± 0.11	unconstrained

Figure 21. Plot of the sizes of the statistical (red filled circles) and systematic (blue crosses) errorbars for the TEPs studied in this work, versus the stellar masses. The errors are plotted as fractions of M_A and the statistical and systematic errors for each TEP are connected by grey lines.

6 PHYSICAL PROPERTIES OF THE TRANSITING EXTRASOLAR PLANETARY SYSTEMS

The main result of this work is the determination of the basic physical properties of thirty TEPs using homogeneous methods. Detailed results for each TEP are given in the many Tables in the Appendix, and the final results for all systems have been summarised in Tables 5 and 6. The homogeneous nature of these numbers means they are well suited for comparing different TEPs, for planning follow-up observations, and for performing detailed statistical studies.

The masses and radii of the stars considered in this work are plotted in Fig. 23 with both their random and systematic errorbars, and with the empirical mass–radius relation (Paper II) indicated. A striking aspect of Fig. 23 is that for $M_A < 1.2\,M_\odot$ the stars generally stick close to the main sequence, but beyond this point their distribution turns almost vertically upwards. The two exceptions are XO-5, which has a more evolved lower-mass star, and OGLE-TR-L9, which contains a more massive star ($1.4\,M_\odot$).
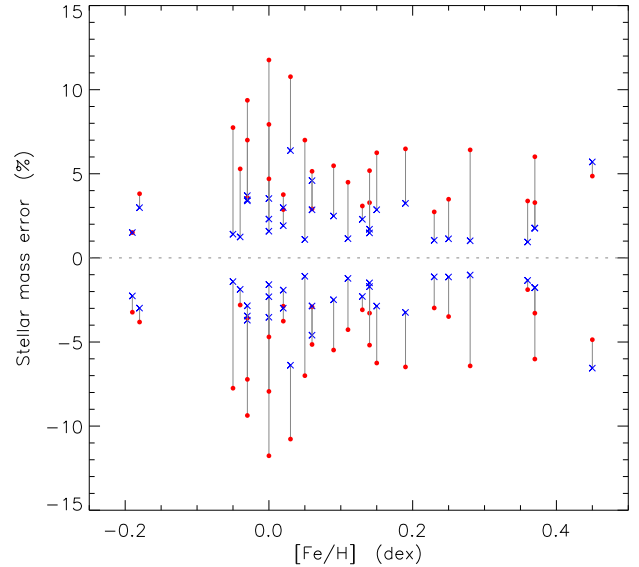
That low-mass stars stick closely to the main sequence is to be expected due to their long evolutionary timescales. The shift to larger R_A at $1.2\,M_\odot$ is reasonable because a larger stellar radius makes it more likely that a given planet is transiting (see Paper II). The avoidance of more massive stars is likely due to difficulty of measuring RVs for these objects, making them lower-priority and more observationally expensive targets for TEP search consortia at

Table 6. Physical properties of the planetary components of the TEPs studied in this work. For each quantity the first uncertainty is derived from a propagation of all observational errors and the second uncertainty is an estimate of the systematic errors arising from the dependence on stellar theory.

System	Mass (M_{Jup})	Radius (R_{Jup})	g_b ($m\,s^{-2}$)	Density (ρ_{Jup})	T'_{eq} (K)	Θ
GJ 436	$0.0737 \pm 0.0051 \pm 0.0018$	$0.365 \pm 0.018 \pm 0.004$	13.7 ± 1.1	$1.51 \pm 0.19 \pm 0.02$	669 ± 22	$0.0253 \pm 0.0015 \pm 0.0003$
HAT-P-1	$0.524 \pm 0.016 \pm 0.008$	$1.217 \pm 0.038 \pm 0.009$	8.77 ± 0.56	$0.290 \pm 0.027 \pm 0.002$	1291 ± 20	$0.0419 \pm 0.0016 \pm 0.0003$
HAT-P-2	$8.74 \pm 0.25 \pm 0.09$	$1.19 \pm 0.12 \pm 0.01$	152 ± 30	$5.1 \pm 1.5 \pm 0.0$	1516 ± 66	$0.771 \pm 0.077 \pm 0.004$
HD 149026	$0.356^{+0.013}_{-0.011}{}^{+0.002}_{-0.003}$	$0.610^{+0.099}_{-0.072}{}^{+0.002}_{-0.003}$	$23.7^{+6.8}_{-6.2}$	$1.57^{+0.72}_{-0.57}{}^{+0.01}_{-0.01}$	1626^{+69}_{-37}	$0.0393^{+0.0054}_{-0.0056}{}^{+0.0002}_{-0.0001}$
HD 189733	$1.150 \pm 0.028 \pm 0.027$	$1.151 \pm 0.036 \pm 0.013$	21.5 ± 1.2	$0.755 \pm 0.066 \pm 0.009$	1191 ± 20	$0.0747 \pm 0.0024 \pm 0.0009$
HD 209458	$0.714 \pm 0.014 \pm 0.009$	$1.380 \pm 0.015 \pm 0.009$	9.30 ± 0.08	$0.272 \pm 0.004 \pm 0.002$	1459 ± 12	$0.0427 \pm 0.0005 \pm 0.0003$
OGLE-TR-10	$0.68 \pm 0.15 \pm 0.00$	$1.72 \pm 0.11 \pm 0.01$	5.7 ± 1.4	$0.134 \pm 0.038 \pm 0.000$	1702 ± 54	$0.0279 \pm 0.0062 \pm 0.0001$
OGLE-TR-56	$1.300 \pm 0.080 \pm 0.010$	$1.20 \pm 0.17 \pm 0.00$	22.3 ± 6.7	$0.75 \pm 0.34 \pm 0.34$	2140 ± 120	$0.0418 \pm 0.0065 \pm 0.0002$
OGLE-TR-111	$0.54 \pm 0.10 \pm 0.01$	$1.077 \pm 0.072 \pm 0.012$	11.5 ± 2.5	$0.43 \pm 0.11 \pm 0.00$	1034 ± 28	$0.056 \pm 0.011 \pm 0.001$
OGLE-TR-113	$1.24 \pm 0.17 \pm 0.02$	$1.111 \pm 0.049 \pm 0.011$	25.0 ± 3.7	$0.91 \pm 0.16 \pm 0.01$	1355 ± 35	$0.0664 \pm 0.0090 \pm 0.0007$
OGLE-TR-132	$1.17 \pm 0.14 \pm 0.01$	$1.25 \pm 0.16 \pm 0.01$	18.5 ± 5.0	$0.59 \pm 0.24 \pm 0.00$	2017 ± 97	$0.0436 \pm 0.0072 \pm 0.0003$
OGLE-TR-182	$1.06 \pm 0.15 \pm 0.01$	$1.47 \pm 0.14 \pm 0.01$	12.1 ± 2.9	$0.332 \pm 0.111 \pm 0.002$	1550 ± 81	$0.0628 \pm 0.0109 \pm 0.0004$
OGLE-TR-211	$0.75^{+0.15}_{-0.15}{}^{+0.01}_{-0.01}$	$1.262^{+0.158}_{-0.091}{}^{+0.005}_{-0.005}$	$11.6^{+2.9}_{-3.3}$	$0.372^{+0.117}_{-0.132}{}^{+0.002}_{-0.001}$	1686^{+90}_{-55}	$0.0460^{+0.0097}_{-0.0104}{}^{+0.0002}_{-0.0002}$
OGLE-TR-L9	$4.34 \pm 1.47 \pm 0.05$	$1.614 \pm 0.083 \pm 0.009$	41 ± 14	$1.03 \pm 0.37 \pm 0.01$	2039 ± 51	$0.153 \pm 0.052 \pm 0.001$
TrES-1	$0.761 \pm 0.045 \pm 0.023$	$1.099 \pm 0.031 \pm 0.017$	15.6 ± 1.2	$0.573 \pm 0.056 \pm 0.009$	1147 ± 15	$0.0612 \pm 0.0037 \pm 0.0009$
TrES-2	$1.253 \pm 0.047 \pm 0.024$	$1.261 \pm 0.039 \pm 0.012$	19.5 ± 1.1	$0.625 \pm 0.051 \pm 0.006$	1467 ± 27	$0.0688 \pm 0.0024 \pm 0.0007$
TrES-3	$1.910^{+0.060}_{-0.070}{}^{+0.020}_{-0.029}$	$1.305^{+0.027}_{-0.025}{}^{+0.007}_{-0.010}$	$27.8^{+1.2}_{-1.4}$	$0.860^{+0.050}_{-0.057}{}^{+0.007}_{-0.004}$	1630^{+23}_{-22}	$0.0719^{+0.0026}_{-0.0026}{}^{+0.0006}_{-0.0004}$
TrES-4	$0.877 \pm 0.072 \pm 0.010$	$1.81 \pm 0.15 \pm 0.01$	6.7 ± 1.2	$0.148 \pm 0.039 \pm 0.001$	1861 ± 54	$0.0373 \pm 0.0042 \pm 0.0002$
WASP-1	$0.860^{+0.072}_{-0.072}{}^{+0.006}_{-0.006}$	$1.484^{+0.059}_{-0.091}{}^{+0.005}_{-0.006}$	$9.7^{+1.5}_{-1.1}$	$0.263^{+0.058}_{-0.036}{}^{+0.001}_{-0.001}$	1800^{+32}_{-49}	$0.0363^{+0.0038}_{-0.0033}{}^{+0.0001}_{-0.0001}$
WASP-2	$0.847 \pm 0.038 \pm 0.024$	$1.043 \pm 0.029 \pm 0.015$	19.32 ± 0.80	$0.747 \pm 0.047 \pm 0.010$	1281 ± 21	$0.0613 \pm 0.0021 \pm 0.0009$
WASP-3	$2.06 \pm 0.13 \pm 0.03$	$1.454 \pm 0.083 \pm 0.009$	24.2 ± 2.6	$0.67 \pm 0.11 \pm 0.00$	2028 ± 59	$0.0715 \pm 0.0048 \pm 0.0004$
WASP-4	$1.237^{+0.059}_{-0.062}{}^{+0.028}_{-0.023}$	$1.357^{+0.033}_{-0.033}{}^{+0.015}_{-0.013}$	$16.65^{+0.26}_{-0.33}$	$0.495^{+0.015}_{-0.018}{}^{+0.005}_{-0.006}$	1661^{+30}_{-30}	$0.0460^{+0.0012}_{-0.0013}{}^{+0.0004}_{-0.0005}$
WASP-5	$1.565 \pm 0.058 \pm 0.026$	$1.164 \pm 0.056 \pm 0.009$	28.7 ± 2.6	$0.99 \pm 0.14 \pm 0.01$	1732 ± 41	$0.0726 \pm 0.0035 \pm 0.0006$
WASP-10	$3.16 \pm 0.23 \pm 0.13$	$1.067 \pm 0.064 \pm 0.022$	68.9 ± 6.7	$2.60 \pm 0.39 \pm 0.05$	972 ± 31	$0.298 \pm 0.019 \pm 0.006$
WASP-18	$10.29 \pm 0.33 \pm 0.16$	$1.158 \pm 0.054 \pm 0.009$	190 ± 16	$6.64 \pm 0.90 \pm 0.05$	2392 ± 51	$0.288 \pm 0.014 \pm 0.002$
XO-1	$0.924 \pm 0.075 \pm 0.019$	$1.206 \pm 0.039 \pm 0.012$	15.8 ± 1.5	$0.526 \pm 0.063 \pm 0.005$	1210 ± 16	$0.0730 \pm 0.0062 \pm 0.0007$
XO-2	$0.555^{+0.062}_{-0.057}{}^{+0.021}_{-0.025}$	$0.992^{+2.1}_{-0.057}{}^{}_{-0.022}$	$14.0^{+2.1}_{-1.5}$	$0.569^{+0.119}_{-0.072}{}^{+0.013}_{-0.011}$	1328^{+17}_{-28}	$0.0432^{+0.0049}_{-0.0045}{}^{+0.0010}_{-0.0008}$
XO-3	$11.83 \pm 0.31 \pm 0.23$	$1.248 \pm 0.047 \pm 0.012$	188 ± 13	$6.08 \pm 0.67 \pm 0.06$	1729 ± 34	$0.711 \pm 0.027 \pm 0.007$
XO-4	$1.521^{+0.160}_{-0.153}{}^{+0.012}_{-0.019}$	$1.29^{+0.38}_{-0.06}{}^{+0.01}_{-0.01}$	$22.8^{+3.2}_{-9.5}$	$0.71^{+0.13}_{-0.40}{}^{+0.01}_{-0.00}$	1630^{+169}_{-36}	$0.1006^{+0.0112}_{-0.0253}{}^{+0.0006}_{-0.0004}$
XO-5	$1.084 \pm 0.055 \pm 0.008$	$1.089 \pm 0.082 \pm 0.004$	22.7 ± 3.2	$0.84 \pm 0.18 \pm 0.00$	1203 ± 33	$0.1075 \pm 0.0082 \pm 0.0004$

Table 4. Physical properties of the WASP-11 / HAT-P-14 system determined by the two discovery papers. Aside from the orbital period, quantities without uncertainties were calculated from the results given in the respective papers.

Parameter	West et al. (2009)	Bakos et al. (2009)
P_{orb} (d)	3.722465	3.7224747
T_{eff} (K)	4800 ± 100	4980 ± 60
$V_{\sin i}$ ($km\,s^{-1}$)	< 6	0.5 ± 0.2
$\left[\frac{M}{H}\right], \left[\frac{Fe}{H}\right]$ (dex)	0.0 ± 0.2	0.13 ± 0.08
K_A ($m\,s^{-1}$)	82.1 ± 7.4	74.5 ± 1.8
e	0 fixed	0 fixed
a (AU)	0.043 ± 0.002	0.0435 ± 0.0006
r_A	0.0801	0.0842 ± 0.0019
r_b	0.01011	0.01104
k	$0.1273^{+0.0011}_{-0.0008}$	0.1313 ± 0.0010
i (°)	$89.8^{+0.2}_{-0.8}$	$88.6^{+0.5}_{-0.4}$
M_A ($M_\odot$)	$0.77^{+0.10}_{-0.08}$	0.83 ± 0.03
R_A ($R_\odot$)	$0.74^{+0.04}_{-0.03}$	0.79 ± 0.02
$\log g_A$ [cgs]	4.45 ± 0.2	4.56 ± 0.02
M_b (M_{Jup})	0.53 ± 0.07	0.460 ± 0.028
R_b (R_{Jup})	$0.91^{+0.06}_{-0.03}$	$1.005^{+0.032}_{-0.027}$
g_b ($m\,s^{-2}$)	$14.5^{+1.4}_{-1.6}$	12.0 ± 0.8
ρ_b (ρ_{Jup})	$0.69^{+0.07}_{-0.11}$	0.479 ± 0.042
T'_{eq} (K)	960 ± 70	1020 ± 17

Figure 22. Same as Fig. 21, except that the error sizes are plotted versus stellar $\left[\frac{Fe}{H}\right]$ rather than mass.

the follow-up stage. There may be a large and presently neglected population of TEPs around more massive stars[11].

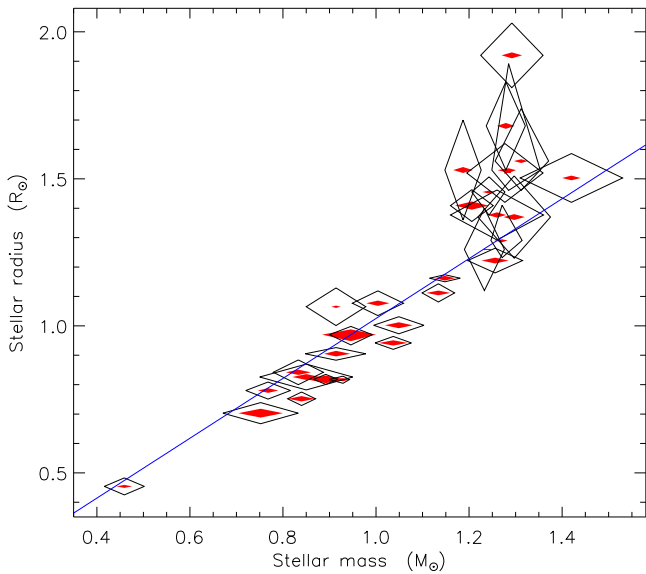[11] Whilst RV surveys mostly concentrate on F, G and K stars, they have

Figure 23. Plot of the masses versus the radii of the stars in the thirty TEPs studied in this work. The statistical uncertainties are shown by black open diamonds and the systematic uncertainties by red filled diamonds. The empirical mass–radius relation from Paper I is shown with a blue line.
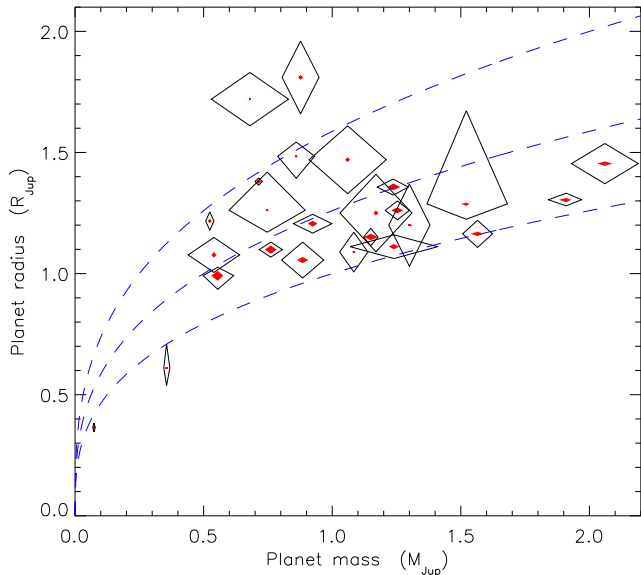

Figure 24. Plot of the masses versus the radii of the planets in the thirty TEPs studied in this work. The statistical uncertainties are shown by black open diamonds and the systematic uncertainties by red filled diamonds. Blue dotted lines show where density is 1.0, 0.5 and 0.25 $\rho_{\rm Jup}$.

Another notable feature of Fig. 23 is that the systematic errors (red filled diamonds in the Figure) are not negligible compared to the random errors, and in some cases (HD 189733, TrES-1, TrES-3, XO-2) are of a similar size or even larger.

A similar diagram for the planets (Fig. 24) shows a much larger scatter in the planet properties, but also that systematic er-

not been neglecting ones more massive than this; see Galland et al. (2005), Johnson et al. (2007) Lagrange et al. (2009) and Bowler et al. (2010).

Figure 25. Mass–radius plot for the known transiting extrasolar planets. Those objects studied in this work are shown with (blue) filled circles and numbers taken from the literature with (red) crosses. The four gas giant planets in our Solar System are denoted with (black) filled circles. Dotted lines show loci where density equals 1.0, 0.5 and 0.25 $\rho_{\rm Jup}$.

rors are much less important for these objects. The two outliers with very low densities are OGLE-TR-10 and TrES-4.

6.1 Physical properties of all known TEPs

The physical properties of the thirty TEPs studied in this work have been augmented with the literature values for the other 41 known systems (as of 31/05/2010) to yield a larger but inhomogeneous sample. Fig. 25 shows their masses and radii on logarithmic axes, alongside those of the four Solar system gas giants. The dominant population of known TEPs continues to reside in a cloud of points centred roughly on $1.0\,\rm M_{\rm Jup}$ and $1.2\,\rm R_{\rm Jup}$. There is a clear tail of high-mass planets, culminating in the brown dwarf CoRoT-3, as well as an increasing number of systems of much smaller mass and radius, typified by GJ 1214 and the first possible rocky exoplanet, CoRoT-7.

Correlations have previously been noticed between $P_{\rm orb}$ and $g_{\rm b}$ (Southworth et al. 2007b) and $P_{\rm orb}$ and $M_{\rm b}$ (Mazeh et al. 2005). The relevant plots are shown in Figs. 26 and 27. In both cases there are ten planets whose properties put them outside the range of $P_{\rm orb}$ shown in these Figures. Neglecting this population of massive planets (which may be a fundamentally different population to the lower mass ones; Fabrycky & Winn 2009; Southworth et al. 2009c), the rank correlation test of Spearman (1904) returns a probability of 99.80% (3.1σ) that the $P_{\rm orb}$–$g_{\rm b}$ correlation is real and 97.6% (2.3σ) that the $P_{\rm orb}$–$M_{\rm b}$ correlation is real. The corresponding figures from Paper II, based on 44 TEPs, are 98.3% and 97.5%. Two concerns with these correlations are apparent. Firstly, they are insignificant if the longer-period planets are not rejected[12]. Secondly, the period–mass correlation has not increased in significance with the addition of 21 new TEPs since Paper II.

Hansen & Barman (2007) divided up eighteen of the twenty

---

[12] Merrill's theorem should be borne in mind: "When one throws away discrepant results, the remainder are found to agree well."
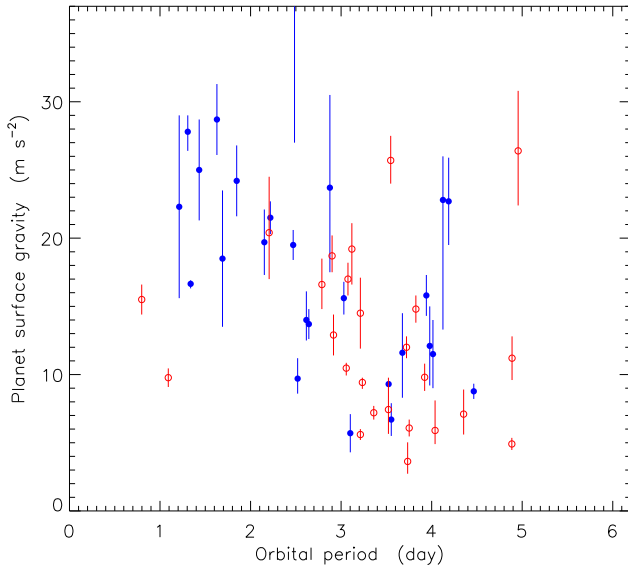
Figure 26. Plot of the orbital periods versus the surface gravities of known TEPs. The objects studied in this work are shown with (blue) filled circles and other objects with (red) open circles.
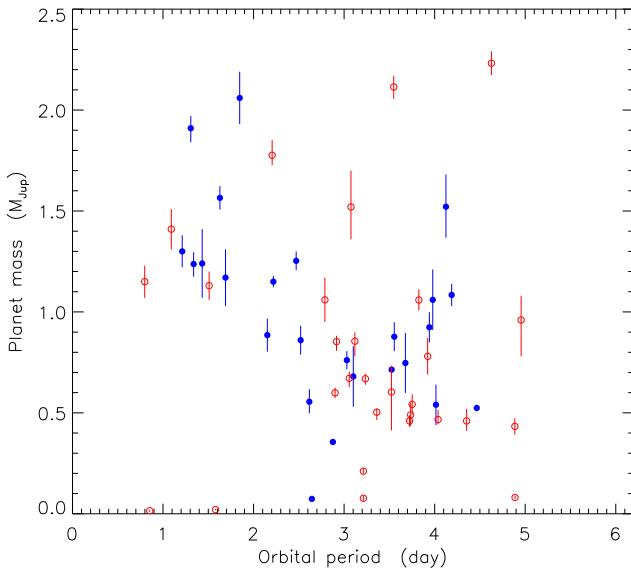

Figure 27. Same as Fig. 26, but for planetary mass instead of $g_{\rm b}$.

TEPs then known into two classes based on their position in a diagram of Θ versus $T_{\rm eq}$. An updated version of the diagram can be seen in Fig. 28, and agrees with previous conclusions (Paper II) that the division between the classes was blurred into insignificance. A dotted line at $\Theta = 0.055$ has been drawn to show the expected boundaries between Class I ($\Theta \approx 0.07 \pm 0.01$) and Class II ($\Theta \approx 0.04 \pm 0.01$). There are several other equally possible lines which could be drawn through this diagram, which does not inspire confidence in their reality. It is probable that the addition of new TEPs in the future will fill out this diagram with objects drawn from a single distribution.

Figure 28. Plot of equilibrium temperature versus Safronov number for the full sample of planets. Objects shown with (blue) circles were studied in this work; those which are just (red) errorbars were not. The dotted line shows the separation between Class A and Class B proposed by Hansen & Barman (2007).

7 SUMMARY

Measurements of the physical properties of many transiting extrasolar planets are available in the literature, but are not directly comparable as they have been derived by different researchers using a variety of methods. In this series of papers I aim to derive the physical properties of the known TEPs using a rigorous and homogeneous approach, resulting in quantities which are suitable for statistical analysis. Each TEP is tackled in two steps, the first being analysis of its transit light curves and the second being the determination of its physical properties.

The transit light curves are studied using the JKTEBOP code, which models binary systems using biaxial spheroids. I pay special attention to the limb darkening of the parent star; solutions are obtained for every light curve using each of five different limb darkening laws. Orbital eccentricity is accounted for by including e and ω as fitted parameters constrained by values and uncertainties measured from radial velocity observations of the parent star. Parameter errors are assessed using Monte Carlo simulations, a residual-permutation algorithm, and the inter-agreement between solutions with different limb darkening laws.

In this paper I present analyses of published transit light curves of fifteen TEPs (Table 2). Three of these (TrES-2, TrES-4 and WASP-2) have faint companion stars within $1.6''$ on the sky (Daemgen et al. 2009). If neglected, this 'third light' dilutes the transit depth and causes systematic errors in parameters measured from the light curves. As a guideline, $L_3 = 5\%$ causes the radius of a representative planet to be underestimated by 2%. I show that it is not possible to detect third light in synthetic light curves representative of good ground-based observations. A third light value must instead be measured and used to constrain the light curve solutions.

In the second stage of the analysis of each TEP, I augment the light curve results with measurements of the velocity amplitude, $T_{\rm eff}$ and $\left[\frac{\rm Fe}{\rm H}\right]$ for its parent star. I then interpolate within tabulated predictions from theoretical stellar models to find the overall best-fitting physical properties of the star and the planet. This

Table 7. Summary of which types of additional observations would be useful for the thirty TEPs studied in this series of papers. ⋆ denotes where additional data would be useful, and ⋆⋆ indicates where it would be useful but difficult to either obtain or interpret.

System	Photometric observations	Radial velocities	Spectral synthesis
GJ 436			⋆⋆
HAT-P-1	⋆		
HAT-P-2	⋆⋆		
HD 149026	⋆		
HD 189733			
HD 209458			
OGLE-TR-10	⋆⋆	⋆⋆	
OGLE-TR-56	⋆⋆	⋆⋆	
OGLE-TR-111		⋆⋆	
OGLE-TR-113	⋆⋆	⋆⋆	⋆
OGLE-TR-132	⋆⋆	⋆⋆	
OGLE-TR-182	⋆⋆	⋆⋆	
OGLE-TR-211	⋆⋆	⋆⋆	
OGLE-TR-L9	⋆	⋆⋆	
TrES-1	⋆	⋆	
TrES-2			
TrES-3			
TrES-4	⋆	⋆	
WASP-1	⋆	⋆	
WASP-2			
WASP-3		⋆	
WASP-4			
WASP-5	⋆		
WASP-10	⋆		⋆
WASP-18	⋆		
XO-1	⋆	⋆	
XO-2		⋆	
XO-3			⋆
XO-4	⋆	⋆	
XO-5	⋆		⋆

model dependence causes systematic errors in the resulting quantities, which I assess by comparing the individual results found using five independent sets of theoretical model predictions. This leads also to 'consensus values' for the physical properties; the Yonsei-Yale models are overall the closest to this consensus.

Measurements of three physical properties are exempt from this model dependence: the planetary surface gravity can be determined from only observed quantities; the density of the star has only a negligible dependence on stellar models; and the planet's equilibrium temperature does not depend on stellar models but does rest on the effective temperature scale of low-mass (F, G and K) stars. The model dependence specifies a minimum level of uncertainty for other physical properties, and this ranges from 1% for M_A to 0.6% for M_b and 0.3% for R_A, R_b and a. Reducing these minimum levels will require improvements in our understanding of low-mass stars. An external test of systematic errors was obtained by comparing the discovery papers of the WASP-11 / HAT-P-10 system. The agreement between the two studies is good for most parameters, but less so for the transit depth and the stellar $T_{\rm eff}$.

Tables 5 and 6 summarise the physical properties of thirty TEPs: the fifteen with light curve analyses in the current work plus another fifteen with photometric analyses in Paper I and later works. The statistical errors in these quantities are calculated using a perturbation analysis which returns complete error budgets for each output parameter. These error budgets indicate which type of follow-up observations are the best way of improving the parameter measurements for each TEP. In most the quality of the light curve is the primary limitation on measurements of the properties of the planet; many systems would also benefit from additional spectroscopic observations. This is summarised in Table 7 for the benefit of follow-up programmes.

The measured properties of the 30 TEPs were then reinforced with those of the other 35 known objects and plotted in several parameter diagrams. I find that the correlation between orbital period and planetary surface gravity is significant at the 3.1σ level once clear outliers are thrown out – this significance has increased with the addition of new systems since Paper II. The period vs. planetary mass correlation has a significance of only 2.3σ, and this *not* increased since Paper II. Similarly, the distinction between Class I and Class II planets in the $T'_{\rm eq}$ vs. Θ diagram is blurring into irrelevance.

In this work I have now treated 30 TEPs, including all currently known from the OGLE, TrES and XO surveys. The discovery rate of transiting planets is expected to continue rising, as the ground-based surveys HAT and WASP mature and new areas of parameter space are probed by the space missions CoRoT and *Kepler*. A homogeneous study of the atmospheric parameters of all TEP host stars would be very complementary to this work. Whilst the light curves obtained by CoRoT and *Kepler* are of extremely high quality, it should not be forgotten that extensive velocity observations are also needed to study transiting systems in detail. Precise physical properties of transiting planets are a fundamental requirement of constraining the atmospheric characteristics, formation and evolution of planetary systems.

REFERENCES

Alonso, R., et al., 2004, ApJ, 613, L153
Ammler-von Eiff, M., Santos, N. C., Sousa, S. G., Fernandes, J., Guillot, T., Israelian, G., Mayor, M., Melo, C., 2009, A&A, 507, 523
Anderson, D. R., et al., 2008, MNRAS, 387, L4
Bakos, G., Noyes, R. W., Kovács, G., Stanek, K. Z., Sasselov, D. D., Domsa, I., 2004, PASP, 116, 266
Bakos, G. Á., Lázár, J., Papp, I., Sári, P., Green, E. M., 2002, PASP, 114, 974
Bakos, G. Á., et al., 2007a, ApJ, 656, 552
Bakos, G. Á., et al., 2007b, ApJ, 670, 826

Bakos, G. Á., et al., 2009, apJ, 696, 1950

Ballard, S., et al., 2009, in Transiting planets, vol. 253 of *IAU Symposium*, p. 470

Bean, J. L., Benedict, G. F., Endl, M., 2006, ApJ, 653, L65

Boisse, I., et al., 2009, A&A, 495, 959

Bonfils, X., Delfosse, X., Udry, S., Santos, N. C., Forveille, T., Ségransan, D., 2005, A&A, 442, 635

Bouchy, F., Pont, F., Santos, N. C., Melo, C., Mayor, M., Queloz, D., Udry, S., 2004, A&A, 421, L13

Bouchy, F., Pont, F., Melo, C., Santos, N. C., Mayor, M., Queloz, D., Udry, S., 2005a, A&A, 431, 1105

Bouchy, F., et al., 2005b, A&A, 444, L15

Bowler, B. P., et al., 2010, ApJ, 709, 396

Bruntt, H., Southworth, J., Torres, G., Penny, A. J., Clausen, J. V., Buzasi, D. L., 2006, A&A, 456, 651

Burke, C. J., et al., 2007, ApJ, 671, 2115

Burke, C. J., et al., 2008, ApJ, 686, 1331

Christian, D. J., et al., 2009, MNRAS, 392, 1585

Claret, A., 2000, A&A, 363, 1081

Claret, A., 2004a, A&A, 428, 1001

Claret, A., 2004b, A&A, 424, 919

Claret, A., 2005, A&A, 440, 647

Claret, A., 2006, A&A, 453, 769

Claret, A., 2007, A&A, 467, 1389

Claret, A., Hauschildt, P. H., 2003, A&A, 412, 241

Collier Cameron, A., et al., 2007, MNRAS, 380, 1230

Daemgen, S., Hormuth, F., Brandner, W., Bergfors, C., Janson, M., Hippler, S., Henning, T., 2009, A&A, 498, 567

Damasso, M., Calcidese, P., Bernagozzi, A., Bertolini, E., Giacobbe, P., Lattanzi, M. G., Smart, R., Sozzetti, A., 2009, in "Pathways towards habitable planets" conference, in press, `arXiv:0911.3587`

Demarque, P., Woo, J.-H., Kim, Y.-C., Yi, S. K., 2004, ApJS, 155, 667

Díaz, R. F., et al., 2007, ApJ, 660, 850

Dittmann, J. A., Close, L. M., Scuderi, L. J., Morris, M. D., 2010, ApJ, submitted, `arXiv:1003.1762`

Dotter, A., Chaboyer, B., Jevremović, D., Kostov, V., Baron, E., Ferguson, J. W., 2008, ApJS, 178, 89

Etzel, P. B., 1981, in Carling, E. B., Kopal, Z., eds., Photometric and Spectroscopic Binary Systems, NATO ASI Ser. C., 69, Kluwer, Dordrecht, p. 111

Fabrycky, D. C., Winn, J. N., 2009, ApJ, 696, 1230

Fernandez, J. M., Holman, M. J., Winn, J. N., Torres, G., Shporer, A., Mazeh, T., Esquerdo, G. A., Everett, M. E., 2009, AJ, 137, 4911

Fortney, J. J., Lodders, K., Marley, M. S., Freedman, R. S., 2008, ApJ, 678, 1419

Galland, F., Lagrange, A., Udry, S., Chelli, A., Pepe, F., Queloz, D., Beuzit, J., Mayor, M., 2005, A&A, 443, 337

Ghezzi, L., Cunha, K., de Araújo, F. X., Smith, V. V., de la Reza, R., Schuler, S., 2010, in K. Cunha, M. Spite, & B. Barbuy, ed., IAU Symposium, vol. 265, p. 432

Gibson, N. P., et al., 2008, A&A, 492, 603

Gibson, N. P., et al., 2009, ApJ, 700, 1078

Gilliland, R. L., et al., 2010, ApJ Letters, in press, `arXiv:1001.0142`

Gillon, M., Pont, F., Moutou, C., Bouchy, F., Courbin, F., Sohy, S., Magain, P., 2006, A&A, 459, 249

Gillon, M., et al., 2007, A&A, 466, 743

Gillon, M., et al., 2009, A&A, 496, 259

Greiner, J., et al., 2008, PASP, 120, 405

Hansen, B. M. S., Barman, T., 2007, ApJ, 671, 861

Hébrard, G., et al., 2008, A&A, 488, 763

Hellier, C., et al., 2009, Nature, 460, 1098

Hilditch, R. W., 2001, An Introduction to Close Binary Stars, Cambridge University Press, Cambridge, UK

Holman, M. J., et al., 2007, ApJ, 664, 1185

Jenkins, J. M., Caldwell, D. A., Borucki, W. J., 2002, ApJ, 564, 495

Johns-Krull, C. M., et al., 2008, ApJ, 677, 657

Johnson, J. A., Winn, J. N., Albrecht, S., Howard, A. W., Marcy, G. W., Gazak, J. Z., 2009a, PASP, 121, 1104

Johnson, J. A., Winn, J. N., Cabrera, N. E., Carter, J. A., 2009b, ApJ, 692, L100

Johnson, J. A., et al., 2007, ApJ, 665, 785

Johnson, J. A., et al., 2008, ApJ, 686, 649

Kipping, D. M., 2008, MNRAS, 389, 1383

Knutson, H. A., Charbonneau, D., Burrows, A., O'Donovan, F. T., Mandushev, G., 2009, ApJ, 691, 866

Koch, D. G., et al., 2010, ApJ, in press, `arXiv:1001.0268`

Konacki, M., Torres, G., Sasselov, D. D., Jha, S., 2005, ApJ, 624, 372

Konacki, M., et al., 2004, ApJ, 609, L37

Krejcova, T., Budaj, J., Krushevska, V., 2010, Communications in Asteroseismology, submitted, `arXiv:1003.1301`

Kurucz, R., 1993, ATLAS9 stellar atmosphere programs and 2 km/s grid. Kurucz CD-ROM No. 13

Kurucz, R. L., 1979, ApJS, 40, 1

Lagrange, A., Desort, M., Galland, F., Udry, S., Mayor, M., 2009, A&A, 495, 335

Loeillet, B., et al., 2008, A&A, 481, 529

Mamajek, E. E., Hillenbrand, L. A., 2008, ApJ, 687, 1264

Mandushev, G., et al., 2007, ApJ, 667, L195

Maness, H. L., Marcy, G. W., Ford, E. B., Hauschildt, P. H., Shreve, A. T., Basri, G. B., Butler, R. P., Vogt, S. S., 2007, PASP, 119, 90

Mayor, M., Queloz, D., 1995, Nature, 378, 355

Mazeh, T., Zucker, S., Pont, F., 2005, MNRAS, 356, 955

McCullough, P. R., et al., 2006, ApJ, 648, 1228

McCullough, P. R., et al., 2008, ApJ, submitted, `arXiv:0805.2921`

Mislis, D., Schmitt, J. H. M. M., 2009, A&A, 500, L45

Mislis, D., Schroter, S., Schmitt, J. H. M. M., Cordes, O., Reif, K., 2009, A&A, in press, `arXiv:0912.4428`

Moutou, C., Pont, F., Bouchy, F., Mayor, M., 2004, A&A, 424, L31

Moutou, C., et al., 2007, A&A, 473, 651

Naef, D., Mayor, M., Beuzit, J. L., Perrier, C., Queloz, D., Sivan, J. P., Udry, S., 2004, A&A, 414, 351

Nelson, B., Davis, W. D., 1972, ApJ, 174, 617

O'Donovan, F. T., et al., 2006, ApJ, 651, L61

O'Donovan, F. T., et al., 2007, ApJ, 663, L37

Pál, A., et al., 2009, ApJ, 700, 783

Pál, A., et al., 2010, MNRAS, 401, 2665

Pietrinferni, A., Cassisi, S., Salaris, M., Castelli, F., 2004, ApJ, 612, 168

Pollacco, D., et al., 2008, MNRAS, 385, 1576

Pollacco, D. L., et al., 2006, PASP, 118, 1407

Pont, F., Bouchy, F., Queloz, D., Santos, N. C., Melo, C., Mayor, M., Udry, S., 2004, A&A, 426, L15

Pont, F., et al., 2007, A&A, 476, 1347

Pont, F., et al., 2008, A&A, 487, 749

Popper, D. M., Etzel, P. B., 1981, AJ, 86, 102

Rabus, M., Deeg, H. J., Alonso, R., Belmonte, J. A., Almenara, J. M., 2009, A&A, 508, 1011

Safronov, V. S., 1972, Evolution of the Protoplanetary Cloud and Formation of the Earth and Planets (Jerusalem: Israel Program for Scientific Translation)

Santos, N. C., Israelian, G., Mayor, M., 2004, A&A, 415, 1153

Santos, N. C., et al., 2006, A&A, 458, 997

Sato, B., et al., 2005, ApJ, 633, 465

Scuderi, L. J., Dittmann, J. A., Males, J. R., Green, E. M., Close, L. M., 2009, ApJ submitted, `arXiv:0907.1685`

Seager, S., Mallén-Ornelas, G., 2003, ApJ, 585, 1038

Simpson, E. K., et al., 2009, MNRAS, submitted, `arXiv:0912.3643`

Skumanich, A., 1972, ApJ, 171, 565

Snellen, I. A. G., Covino, E., 2007, MNRAS, 375, 307

Snellen, I. A. G., et al., 2009, A&A, 497, 545

Southworth, J., 2008, MNRAS, 386, 1644 (Paper I)

Southworth, J., 2009, MNRAS, 394, 272 (Paper II)

Southworth, J., Maxted, P. F. L., Smalley, B., 2004a, MNRAS, 349, 547

Southworth, J., Maxted, P. F. L., Smalley, B., 2004b, MNRAS, 351, 1277

Southworth, J., Zucker, S., Maxted, P. F. L., Smalley, B., 2004c, MNRAS, 355, 986

Southworth, J., Smalley, B., Maxted, P. F. L., Claret, A., Etzel, P. B., 2005, MNRAS, 363, 529

Southworth, J., Bruntt, H., Buzasi, D. L., 2007a, A&A, 467, 1215

Southworth, J., Wheatley, P. J., Sams, G., 2007b, MNRAS, 379, L11

Southworth, J., et al., 2009a, MNRAS, 396, 1023

Southworth, J., et al., 2009b, MNRAS, 399, 287

Southworth, J., et al., 2009c, ApJ, 707, 167

Southworth, J., et al., 2010, MNRAS submitted

Sozzetti, A., Torres, G., Charbonneau, D., Latham, D. W., Holman, M. J., Winn, J. N., Laird, J. B., O'Donovan, F. T., 2007, ApJ, 664, 1190

Sozzetti, A., et al., 2009, ApJ, 691, 1145

Spearman, C., 1904, American Journal of Psychology, 72

Stempels, H. C., Collier Cameron, A., Hebb, L., Smalley, B., Frandsen, S., 2007, MNRAS, 379, 773

Street, R. A., et al., 2007, MNRAS, 379, 816

Torres, G., Winn, J. N., Holman, M. J., 2008, ApJ, 677, 1324

Triaud, A. H. M. J., et al., 2009, A&A, 506, 377

Triaud, A. H. M. J., et al., 2010, A&A, submitted

Tripathi, A., et al., 2010, ApJ, in press, `arXiv:1004.0692`

Udalski, A., Kubiak, M., Szymański, M., 1997, AcA, 47, 319

Udalski, A., Szewczyk, O., Zebrun, K., Pietrzynski, G., Szymanski, M., Kubiak, M., Soszynski, I., Wyrzykowski, L., 2002, Acta Astronomica, 52, 317

Udalski, A., et al., 2008, A&A, 482, 299

Valenti, J. A., Fischer, D. A., 2005, ApJS, 159, 141

van Belle, G. T., von Braun, K., 2009, ApJ, 694, 1085

Van Hamme, W., 1993, AJ, 106, 2096

VandenBerg, D. A., Bergbusch, P. A., Dowler, P. D., 2006, ApJS, 162, 375

West, R. G., et al., 2009, A&A, 502, 395

Wheatley, P. J., et al., 2010, ApJ, submitted, `arXiv:1004.0836`

Winn, J. N., Holman, M. J., Shporer, A., Fernández, J., Mazeh, T., Latham, D. W., Charbonneau, D., Everett, M. E., 2008a, AJ, 136, 267

Winn, J. N., et al., 2007a, ApJ, 665, L167

Winn, J. N., et al., 2007b, AJ, 133, 1828

Winn, J. N., et al., 2007c, AJ, 134, 1707

Winn, J. N., et al., 2008b, ApJ, 683, 1076

Winn, J. N., et al., 2009, ApJ, 700, 302